

Increases in Future AR Count and Size: Overview of the ARTMIP Tier 2 CMIP5/6 Experiment

T. A. O'Brien^{1,2*}, M. F. Wehner³ and A. E. Payne⁴ and C. A. Shields⁵ and J. J. Rutz⁶ and L.-R. Leung⁷ and F. M. Ralph⁸ and A. Collow^{9,10} and I. Gorodetskaya¹¹ and B. Guan¹² and J. M. Lora¹³ and E. McClenny¹⁴ and K. M. Nardi¹⁵ and A. M. Ramos¹⁶ and R. Tomé¹⁶ and C. Sarangi^{7,18} and E. J. Shearer¹⁷ and P. A. Ullrich¹⁴ and C. Zarzycki¹⁵ and B. Loring³ and H. Huang² and H. A. Inda-Díaz^{14,2} and A. M. Rhoades² and Y. Zhou²

¹Dept. of Earth and Atmospheric Sciences, Indiana University, Bloomington, IN, USA

²Climate and Ecosystem Sciences Division, Lawrence Berkeley National Laboratory, Berkeley, CA, USA

³Computational Research Division, Lawrence Berkeley National Laboratory, Berkeley, CA, USA

⁴Dept. of Earth and Space Sciences, University of Michigan, Ann Arbor, MI, USA

⁵National Center for Atmospheric Research, Boulder, CO, USA

⁶National Weather Service, Western Region Headquarters, Science and Technology Infusion Division, Salt Lake City, UT, USA

⁷Atmospheric Sciences and Global Change Division, Pacific Northwest National Laboratory, Richland, WA, USA

⁸Center for Western Weather and Water Extremes, Scripps Institution of Oceanography, University of California, San Diego, La Jolla, CA, USA

⁹Universities Space Research Association, Columbia, MD, USA

¹⁰Global Modeling and Assimilation Office, NASA Goddard Space Flight Center, Greenbelt, MD, USA

¹¹Centre for Environmental and Marine Studies, Dept. of Physics, University of Aveiro, Portugal

¹²Joint Institute for Regional Earth System Science and Engineering, University of California, Los Angeles, CA, USA

¹³Dept. of Earth and Planetary Sciences, Yale University, New Haven, CT, USA

¹⁴Dept. of Land, Air and Water Resources, University of California, Davis, CA, USA

¹⁵Dept. of Meteorology and Atmospheric Science, Penn State University, University Park, PA, USA

¹⁶Instituto Dom Luiz (IDL), Faculdade de Ciências, Universidade de Lisboa, Lisboa, Portugal

¹⁷Center for Hydrometeorology and Remote Sensing, University of California, Irvine, Irvine, CA, USA

¹⁸Department of Civil Engineering, Indian Institute of Technology Madras, India

Key Points:

- Uncertainty associated with AR definition dominates model uncertainty for projections of Pacific and Atlantic landfalling ARs
- Most AR detection algorithms show an increase in AR frequency in future simulations
- AR statistics in CMIP 5-and-6 models compare remarkably well with reanalysis

*Dept. of Earth and Atmospheric Science, 1001 E. 10th St, Bloomington, IN, 47408

Corresponding author: T.A. O'Brien, obrienta@iu.edu

Abstract

The Atmospheric River (AR) Tracking Method Intercomparison Project (ARTMIP) is a community effort to systematically assess how the uncertainties from AR detectors (ARDTs) impact our scientific understanding of ARs. This study describes the ARTMIP Tier 2 experimental design and initial results using the Coupled Model Intercomparison Project (CMIP) Phases 5 and 6 multi-model ensembles. We show that AR statistics from a given ARDT in CMIP5/6 historical simulations compare remarkably well with the MERRA-2 reanalysis. In CMIP5/6 future simulations, most ARDTs project a global increase in AR frequency, counts, and sizes, especially along the western coastlines of the Pacific and Atlantic oceans. We find that the choice of ARDT is the dominant contributor to the uncertainty in projected AR frequency when compared with model choice. These results imply that new projects investigating future changes in ARs should explicitly consider ARDT uncertainty as a core part of the experimental design.

Plain Language Summary

Atmospheric rivers (ARs) are a type of weather pattern known to be important for moving water vapor from the warm, moist tropics to the cool, dry polar regions; when they reach midlatitudes in the winter time, they are commonly associated with heavy precipitation. Recent studies that assess the impacts of global climate change on ARs tend to agree that there will be more ARs in a warmer climate, and that ARs will tend to be more extreme. However, it has been increasingly recognized by the AR research community that these results may depend on the method used to identify ARs and the choice of climate model. This study reports results from a controlled experiment, involving an international research community, that aims to show how different AR identification methods and climate models might impact our scientific understanding of ARs in the future. This experiment shows that there will likely be more ARs in the future, and that ARs will generally have a larger spatial footprint. This experiment also shows that uncertainty in these results are large, with the uncertainty from AR identification methods outweighing that of climate models. Future efforts to better understand the physics of ARs may help us reduce this uncertainty.

1 Introduction

Over the past 40 years, research on atmospheric rivers (ARs), filamentary bands of intense water vapor transport that were known as tropical cloud plumes in earlier literature, has increasingly demonstrated their importance for cloud and precipitation variability (Thepenir & Cruette, 1981; McGuirk et al., 1987; Lau & Chan, 1988; Kuhnel, 1989; Kiladis & Weickmann, 1992; Rasmusson & Arkin, 1993; Iskenderian, 1995), the global hydrological cycle (Newell et al., 1992; Zhu & Newell, 1998; Ralph et al., 2017) and regional energy and water cycles (Newell & Zhu, 1994; Neiman, Ralph, Wick, Kuo, et al., 2008; Ralph et al., 2005; Dettinger et al., 2011; Gimeno et al., 2016; Gershunov et al., 2017; Shields, Rosenbloom, et al., 2019). ARs are a main source of precipitation and are frequently associated with hydroclimatological impacts in the midlatitude western margins of North America (Neiman et al., 2002; Ralph et al., 2004, 2005; Neiman, Ralph, Wick, Kuo, et al., 2008; Leung & Qian, 2009; Guan et al., 2010; Warner et al., 2012; Neiman et al., 2013; Ralph et al., 2013; Rutz et al., 2014; Huang et al., 2021), South America (Viale & Nuñez, 2011; Gimeno et al., 2016), Europe (Stohl et al., 2008; Lavers et al., 2012; Lavers & Villarini, 2013; Ramos et al., 2015; Gimeno et al., 2016), and South Africa (Blamey et al., 2018; Ramos et al., 2019). AR impacts on surface heat and water mass balance in polar regions are increasingly evident (Newell & Zhu, 1994; Gorodetskaya et al., 2014; Mattingly et al., 2020; Wille et al., 2019, 2021). Increased understanding of ARs has led to improvements in flood forecasting (Lavers, Waliser, et al., 2016; Lavers, Pappenberger,

86 et al., 2016) and in communication of flood-related risks when intense ARs are immi-
87 nent (Ralph, Rutz, et al., 2019).

88 Numerous recent studies have analyzed ARs in future climate scenarios (e.g., Warner
89 et al., 2015; Lavers et al., 2015; Gao et al., 2015a, 2016; Shields & Kiehl, 2016b, 2016a;
90 Polade et al., 2017; Espinoza et al., 2018; Gershunov et al., 2019; Rhoades, Jones, Sri-
91 vastava, et al., 2020; Rhoades et al., 2021) (see Payne et al. (2020) and references therein).
92 Payne et al. (2020) reviews the related studies over the past 10 years and shows that (1)
93 studies generally agree that global increases in atmospheric moisture will increase the
94 intensity of ARs, and that (2) there is wide uncertainty in the results conveyed in the
95 literature, especially in areas outside the well-studied U.S. west coast. Existing studies
96 generally agree that the frequency and intensity of ARs will increase, and some studies
97 indicate poleward shifts of the AR tracks (Sousa et al., 2020; Shearer et al., 2020). Gershunov
98 et al. (2019) show that intermodel differences in future projections of precipitation are
99 much lower when considering precipitation due to ARs than those when considering changes
100 in bulk precipitation. Given that precipitation is produced by a variety of meteorolog-
101 ical phenomena, and that there is no guarantee that the relative proportions of precip-
102 itation from various phenomena are the same in models as they are in observations, Gershunov
103 et al. (2019) highlight the importance in using a phenomenon-focused study of precip-
104 itation in future climate simulations.

105 Essentially all of the studies of ARs and future climate (and past climate, e.g., Lora
106 et al., 2017; Kiehl et al., 2018; Skinner et al., 2020; Menemenlis et al., 2021) rely on ob-
107 jective, quantitative methods to discriminate ARs from the background: AR detectors
108 (ARDTs). At present, ARs have a qualitative definition (Ralph et al., 2018), which leaves
109 researchers with the task of implementing a quantitative definition of ARs in specific ARDTs.
110 ARDTs typically consist of a set of heuristic rules (e.g., thresholds and filters) that fo-
111 cus on identifying anomalously high moisture or moisture transport that occurs in con-
112 tiguous, filamentary structures. The design of ARDTs is guided by understanding gained
113 through decades of observational and model studies (Browning & Pardoe, 1973; McGuirk
114 et al., 1987; Newell et al., 1992; Zhu & Newell, 1998; Lackmann & Gyakum, 1999; Neiman
115 et al., 2002; Ralph et al., 2004, 2005; Bao et al., 2006; Neiman, Ralph, Wick, Kuo, et al.,
116 2008; Neiman, Ralph, Wick, Lundquist, & Dettinger, 2008; Waliser et al., 2012). The
117 number of ARDT algorithms has grown with the number of ARDT studies over the past
118 decade, with new ARDTs often being developed for specialized purposes: e.g., ARDTs
119 for understanding the global hydrological cycle (Zhu & Newell, 1998; Guan & Waliser,
120 2015), observed hydrometeorological extremes (Neiman, Ralph, Wick, Lundquist, & Det-
121 tinger, 2008; Rutz et al., 2014), the cryosphere (Gorodetskaya et al., 2014; Wille et al.,
122 2021), and regional hydroclimate variability (Gershunov et al., 2017). Even though ARDTs
123 are often initially designed with different purposes in mind, Payne et al. (2020) demon-
124 strate that there is overlap in what they are ultimately used to study. The community
125 has recently started to recognize that uncertainty associated with the numerical defini-
126 tion of ARs may have important implications for our understanding of ARs and their
127 changes in a future warmer world (Newman et al., 2012; Huning et al., 2017; Shields et
128 al., 2018; Guan et al., 2018; Rutz et al., 2019; Ralph, Wilson, et al., 2019; Shields, Rutz,
129 et al., 2019; Shields, Rosenbloom, et al., 2019; Lora et al., 2020; O’Brien, Payne, et al.,
130 2020; O’Brien, Risser, et al., 2020)

131 The Atmospheric River Tracking Method Intercomparison Project (ARTMIP) was
132 launched by members of the AR research community in order to systematically assess
133 the impact of this uncertainty on our scientific understanding (Shields et al., 2018). The
134 First ARTMIP Workshop (Shields, Rutz, et al., 2019) defined a multi-tier experimen-
135 tal design focusing on uncertainty in the observational record (Tier 1; Rutz et al., 2019),
136 and uncertainty in AR variability and change (Tier 2). Two Tier 2 experiments were launched
137 at the Second ARTMIP Workshop (Shields, Rutz, et al., 2019): the Tier 2 C20C+ ex-
138 periment and the Tier 2 CMIP5/6 experiment. Both experiments are designed to elu-

139 culate the effect of uncertainty associated with ARDTs on our understanding of ARs,
140 with the former focusing on uncertainty in regional impacts in a single high-resolution
141 global model, and the latter focusing on the relative roles of model and ARDT-associated
142 uncertainty. A third Tier 2 experiment was launched at the Third ARTMIP Workshop:
143 the Tier 2 Reanalysis experiment, which aims to understand how differences across re-
144 analyses compare with differences across ARDTs. This manuscript overviews the Tier
145 2 CMIP5/6 experiment.

146 2 Data and Methods

147 We use data from the ARTMIP Tier 1 experiment (Shields et al., 2018; Rutz et
148 al., 2019), which provides atmospheric river detections from multiple ARDT algorithms.
149 All Tier 1 ARDTs run on a common set of atmospheric fields (e.g., integrated vapor trans-
150 port) derived from the Modern-Era Retrospective analysis for Research and Applications,
151 Version 2 (MERRA-2; Gelaro et al., 2017). A subset of the Tier 1 algorithms have also
152 been run on the Tier 2 input dataset described further on. The subset of algorithms run
153 was determined by the subset of ARTMIP participants who volunteered to run their al-
154 gorithms on the Tier 2 dataset; these algorithms include `ARCONNECT_v2` (Shearer et al.,
155 2020), `Guan_Waliser_v2` (Guan & Waliser, 2015; Guan et al., 2018), `IDL_re1_future`
156 & `IDL_re1_hist` (Ramos et al., 2016; Blamey et al., 2018), `Lora_v2` (Lora et al., 2017;
157 Skinner et al., 2020), `Mundhenk_v3` (Mundhenk et al., 2016), `PNNL_v1` (Hagos et al., 2015),
158 and `TECA-BARD v1.0.1` (O’Brien, Risser, et al., 2020), and `Tempest` (Ullrich & Zarzy-
159 cki, 2017; McClenny et al., 2020) (see Table S1). Text S4 describes why choice of reanal-
160 ysis unlikely affects the qualitative conclusions of this paper.

161 For the Tier 2 input dataset for ARDTs, we derive integrated water vapor (IWV),
162 and the components of the integrated vapor transport (IVT) vector from outputs from
163 atmosphere-ocean general circulation models associated with the Coupled Model Inter-
164 comparison Project (CMIP) 5 (Taylor et al., 2012) and 6 (Eyring et al., 2016; O’Neill
165 et al., 2016) multi-model ensembles (hereafter referred to as CMIP5/6 when both en-
166 sembles are jointly discussed). We utilize model output from the historical simulations
167 in both CMIP5 and CMIP6, and we utilize output from the representative concentra-
168 tion pathway 8.5 (RCP8.5, CMIP5) and shared socioeconomic pathways 5-8.5 experi-
169 ments (SSP5-8.5, CMIP6). We utilize models that provided specific humidity q (`hus`)
170 and wind \vec{u} (`ua` and `va`) at 6-hourly intervals on the native model vertical grid (the `6hrLev`
171 table); we further restrict the set of models to those which provide model output from
172 the same ensemble member for both the historical and future (RCP8.5 and SSP5-8.5)
173 simulations. We chose to focus on models providing data on the native model vertical
174 grid (either sigma or hybrid-sigma) because this facilitates an accurate calculation of ver-
175 tical integrals without having to handle below-ground levels as would be necessary if deal-
176 ing with model output on isobaric surfaces; this choice simplifies interpretation of inter-
177 ARDT differences in continental interiors, where such below-ground levels are common.
178 At the time that the Tier 1 input dataset was constructed (in Summer 2019), we were
179 able to access 6 models from CMIP5 (CCSM4, CSIRO-Mk3-6, CanESM2, IPSL-CM5A-
180 LR, IPSL-CM5B-L, and NorESM1-M) and 3 models from CMIP6 (BCC-CSM2-MR, IPSL-
181 CM6A-LR, MRI-ESM2-0; Xin et al., 2019; Yukimoto et al., 2019; Boucher et al., 2019)
182 that satisfied these constraints (see Table S1): 9 models in total and one ensemble mem-
183 ber from each model. We focus on the 1981-2010 time period for the historical reference
184 period, and we calculate trends over the 1951-2099 period (some data are missing due
185 to data availability and corruption issues, and years with these issues are not included
186 in calculations; see Text S3). Examination of the 1951-2099 timeseries at a variety of lo-
187 cations show that changes in AR frequency are close to linear; therefore the trends pre-
188 sented here can be used to infer discrete changes in AR frequency at arbitrary timepe-
189 riods (e.g., mid-century and end-of-century). The models selected represent a range of
190 horizontal resolutions (ranging from approximately 100 km to 300 km), and the RCP8.5

and SSP5-8.5 scenarios represent aggressive emission trajectories with large amounts of radiative forcing (nominally 8.5 W/m²) by end-of-century.

The mass-weighted vertical integrals of water vapor (ρq) and water vapor transport ($\rho \vec{u} q$) are calculated from all native model levels in the CMIP5/6 output as:

$$\text{IWV} = -\frac{1}{g} \sum_{k=1}^N q_k \Delta p_k \quad (1)$$

$$\overrightarrow{\text{IVT}} = -\frac{1}{g} \left\langle \sum_{k=1}^N u_k q_k \Delta p_k, \sum_{k=1}^N v_k q_k \Delta p_k \right\rangle, \quad (2)$$

where index k corresponds to model levels going from the surface ($k = 1$) to the top of the model atmosphere ($k = N$), and Δp_k is the difference in level pressures, estimated at level k . The total vapor transport is calculated as the vector magnitude: $\text{IVT} = \left| \overrightarrow{\text{IVT}} \right|$.

These ARDTs consist of a mixture of algorithms that detect ARs globally (global algorithms) and algorithms designed for specific regions (regional algorithms); see Table S1. We focus most of the analysis in this manuscript on the location of the AR tracks, changes in these tracks, and uncertainty therein. We therefore focus the bulk of the discussion on the global subset of algorithms; the full set of algorithms is discussed in Section 3.3 when comparing the relative magnitudes of uncertainty related to ARDT design and model choice.

2.1 Tier 2 CMIP5/6 Experiment Overview

All Tier 2 CMIP5/6 ARDT contributions use the common dataset of IWV, IVT, and $\overrightarrow{\text{IVT}}$ described in Section 2, which come from 9 models in the CMIP5 and CMIP6 multi-model ensembles. ARDT outputs are regridded to a common 4°x5° latitude-longitude grid. We assess the CMIP5/6 models by comparing annual spatial patterns of AR frequency between the Tier 1 and Tier 2 experiments, for each detection scheme independently, focusing on spatial pattern correlation and spatial variability. Given the 6-hourly frequency of the dataset, we report frequency as ‘equivalent’ AR days, which we define as 0.25 times the total number of timesteps with AR conditions. We provide details about Tier 2-specific modifications to ARDTs in Text S1 and details about missing data in Text S3.

Grouping algorithms by the type of criteria applied (relative versus absolute thresholds) and degree of restrictiveness (magnitude of thresholds employed, number of criteria involved) can reduce the spread associated with ARDTs (Rutz et al., 2019; Ralph, Wilson, et al., 2019). Here, we group ARDTs into three categories, based on their treatment of thresholds: *absolute* (ARCONNECT_v2, PNNL_v1, and Lora_v2), *fixed relative* (Guan_Waliser_v2, IDL_rel_future, IDL_rel_hist, and Mundhenk_v3), and *relative* (Tempest and TECA-BARD v1.0.1). The categorizations are described and justified in Text S2. A key motivation for this categorization is aggregating ARDTs by their sensitivity to thermodynamic changes in IVT, with the assumption that ARDTs employing absolute thresholds to moisture fields will be the most sensitive, and ARDTs employing time-dependent thresholds will be least sensitive.

3 Results

3.1 Evaluation of Historical Simulations

We show maps of annual average AR frequency from the Tier 1 (MERRA-2) experiments for the 6 global ARDT algorithms in the top row of Figure 1. The ARDTs show broad consistency in the spatial patterns of ARs. All ARDTs identify well-known AR tracks, with distinct maxima in the midlatitude Pacific and the Atlantic, and with a circumglobal maximum in the Southern Ocean; these AR tracks have been described

233 in papers using multiple ARDTs (e.g., Zhu & Newell, 1998; Lavers et al., 2012; Guan
234 & Waliser, 2015; Gimeno et al., 2016; Lora et al., 2020). The ARDTs also identify sig-
235 nificant areas with little or no AR activity: the tropics, northeastern Asia, northeast-
236 ern South America, tropical and subtropical Africa, the subtropical eastern Pacific (near
237 the cold tongue region), as well as interiors of both polar regions (except for with `Guan_Waliser_V2`).
238 The ARDTs differ significantly in the relative frequency of AR conditions. Some of the
239 ARDTs identify AR conditions occurring upwards of 30 days per year (approximately
240 one twelfth of the time) in the main AR tracks, and other ARDTs identify AR condi-
241 tions occurring fewer than 10 days per year. These results are consistent with previous
242 ARDT comparisons, indicating a wide range of restrictiveness across ARDTs (Ralph,
243 Wilson, et al., 2019; Rutz et al., 2019; Lora et al., 2020). The algorithms also differ in
244 the degree to which the AR tracks penetrate inland and the maximum poleward exten-
245 sion of the AR tracks (poleward non-zero AR boundary), with the `Guan_Waliser_v2` al-
246 gorithm commonly identifying ARs in continental interiors and polar regions, and `TECA-BARD v1.0.1`
247 rarely identifying ARs in continental interiors and polar regions. The average frequency
248 of ARs (the top-right panel in Figure 1) exhibits a similar spatial pattern to the vari-
249 ous ARDTs, with ARs occurring approximately 10 days per year in the core AR track.

250 Simulated ARs in the Tier 2 CMIP5/6 experiment are remarkably consistent with
251 those in the Tier 1 MERRA-2 experiment. Results from an arbitrary model-MRI-ESM-
252 2-0 from the CMIP6 multimodel ensemble—are shown in the second row of Figure 1, and
253 a similar plot showing results from all possible model-ARDT pairs is shown in Figure S1.
254 The placement of the AR tracks (and opposing gaps in ARs) are very similar when com-
255 paring spatial maps for a given ARDT. The algorithm-mean AR frequencies (last col-
256 umn) show very little difference between Tier 1 and 2; this is true for all models ana-
257 lyzed (see Figure S1).

258 Each ARDT has idiosyncratic spatial patterns that are expressed in both Tier 1
259 and Tier 2. This suggests that the spatial pattern maps are an emergent property of each
260 ARDT, and that these spatial patterns are relatively insensitive to significant changes
261 in the representation of the underlying atmospheric dynamics. For example, the diffuse
262 spatial pattern associated with the `Guan_Waliser_v2` (GW) algorithm is evident in Tier
263 1 and in all Tier 2 simulations (Figures S1 and S2), and the multi-model mean for the
264 GW algorithm exhibits a similar spatial pattern. This suggests that there is much more
265 variability in AR frequency across ARDT algorithms than there is across simulations;
266 we quantify this in Section 3.3.

267 Figure 2a quantitatively shows that CMIP5 and CMIP6 simulations compare well
268 with the MERRA-2 reanalysis when compared within a single ARDT. Spatial correla-
269 tion coefficients between the AR frequency maps in individual Tier 2 simulations and
270 the corresponding Tier 1 map are above $r = 0.95$ for most ARDT-model pairs (32 out
271 of 52 pairs), and the ratio of spatial standard deviations of AR frequency (Tier 2 divided
272 by Tier 1) is between 0.75 and 1.25 for 40 out of 52 ARDT-model pairs. The Taylor skill
273 scores (Taylor, 2001) are above 0.9 for 37 out of 52 ARDT-model pairs. Variability ex-
274 ists, with some ARDT-model pairs reaching as high as $r \approx 0.97$ and only 5 ARDT-model
275 pairs with correlation coefficients between 0.8 and 0.9 (and skill scores below 0.85); like-
276 wise, one combination (`ARCONNECT_v2` and CMIP5 IPSL-CM5A-LR) has variability that
277 is too low by approximately 25%, and one combination (`Tempest` and CMIP5 IPSL-CM5B-
278 LR) has variability that is about 50% too high. Overall, this emphasizes the high de-
279 gree of similarity between simulated ARs and ARs in MERRA-2, when comparing re-
280 sults using a single ARDT.

281 Altogether, the various ARDTs portray a similar assessment of model skill, with
282 essentially all of the models analyzed appearing to be ‘fit for purpose’. This is true even
283 for the lowest resolution simulations (e.g., CMIP5 CanESM2 with a nominal 310 km hor-
284 izontal resolution in the tropics; see Table S1), which have some of the highest correla-
285 tion coefficients. (Note that the AR detection process was performed at the original model

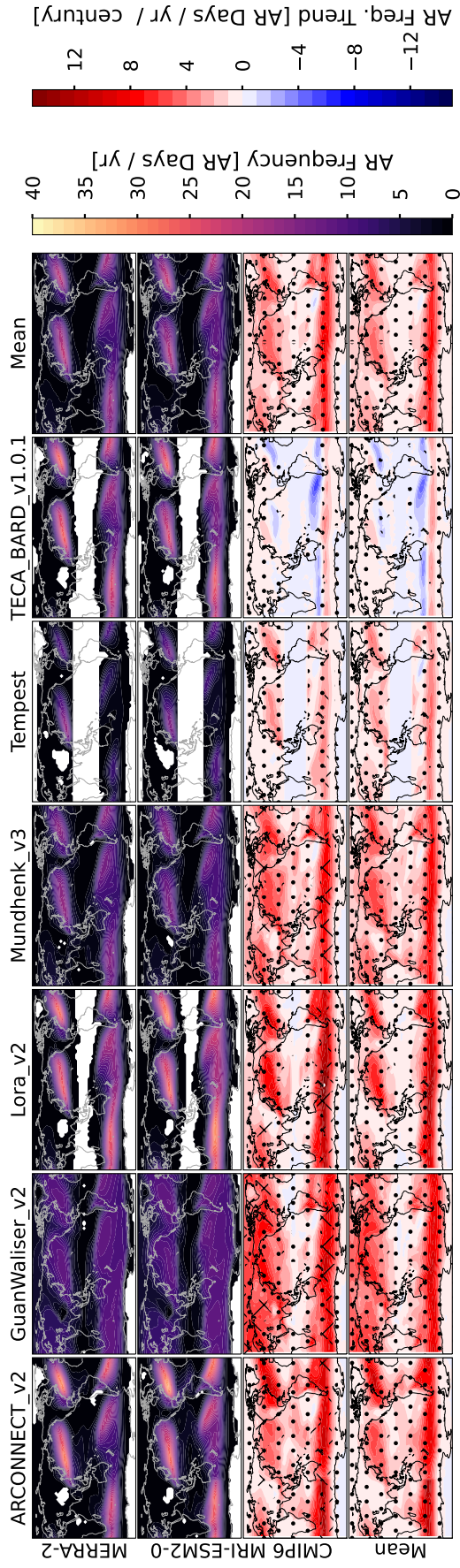


Figure 1. (first and second rows) Maps of AR frequency (shown as average number of days with AR conditions) annually for the 1981-2010 period. Each column corresponds to a global AR detection algorithm, and the last column represents the average across all AR detection algorithms. The top row corresponds to AR detections on the MERRA-2 dataset (the Tier 1 ARTMIP experiment) and the second and third rows correspond to AR detections on the CMIP6 MRI-ESM2-0 simulation. White indicates areas where average AR occurrence is fewer than 1 day. (third and fourth rows) Maps of trends in annual AR frequency in the MRI-ESM2-0 simulation (third row) and all models (fourth row), organized by detection algorithm (columns) from 1951-2099 (with a few exceptions noted in the text). Trends significant at the 90% level (according to a 2-sided t-test) are indicated by stippling, and trends significant at the 95% level are indicated by cross-hatching.

286 resolution, prior to regridding to a common grid for comparison with reanalysis.). A sur-
287 vey of the literature (Gao et al., 2015b; Hagos et al., 2015; Shields & Kiehl, 2016b; Guan
288 & Waliser, 2017; Payne et al., 2020; Reid et al., 2020; Rhoades, Jones, O’Brien, et al.,
289 2020) indicates a mix of possible resolution effects, with some indication that the effect
290 of resolution may depend on the experimental setup (e.g., coupled vs uncoupled; Guan
291 & Waliser, 2017). We hypothesize that resolution effects may depend on the ARDT used;
292 these effects could be studied more systematically by applying multiple ARDTs to the
293 CMIP6 HighResMIP experiment (Haarsma et al., 2016). The ARTMIP community has
294 discussed the possibility of coordinating a Tier 2 Resolution experiment (O’Brien, Payne,
295 et al., 2020) to explore this more systematically.

296 Results associated with the **Tempest** algorithm are a somewhat notable exception:
297 five of the models evaluated with **Tempest** have high spatial variability relative to MERRA-
298 2, and relatively low spatial correlations. This may be related to some differences in the
299 implementation of **Tempest** between the Tier 1 and Tier 2 experiments (see Text S1).

300 3.2 Projected Changes in AR Frequency, Count, and Size

301 When the ARDTs are applied to the various future simulations described in Sec-
302 tion 2, they project a variety of trends in AR frequency. Figure 1 (third row) shows that
303 most ARDTs applied to the MRI-ESM2-0 simulation indicate increases in AR frequency
304 in the main AR tracks. Within each algorithm, the trends from the MRI-ESM2-0 sim-
305 ulation are quantitatively and qualitatively similar to trends from other simulations (see
306 Figure S3), as indicated by the similarity between the MRI-ESM2-0 trends and the multi-
307 model trends shown in the bottom row of Figure 1. The average trend across all model-
308 ARDT combinations (lower right panel of Figure 1) likewise indicates an increase in AR
309 frequency in the midlatitude storm tracks, with increases of ~ 5 AR days per year per
310 century (an approximate 50% increase). In addition to this increase in AR frequency in
311 the mid-latitude storm tracks, it is also important to note an increase in the areas with
312 historically rare or close to zero frequency of the ARs, such as southern Asia and Africa,
313 the Arctic Ocean and the Antarctic ice sheet. There are essentially no ocean basins where
314 the model-ARDT mean indicates a decrease in AR frequency.

315 The climatological pattern of AR frequency is primarily controlled by changes in
316 AR size, AR occurrence (count), and AR location. Two ARDTs (**TECA-BARD v1.0.1** and
317 to a lesser extent **Tempest**) suggest poleward shifts in AR location (Figure 1, bottom row,
318 and Figure S3), whereas **ARCONNECT_v2**, **GuanWaliser_v2**, **Lora_v2**, and **Mundhenk_v3**
319 indicate quasi-global increases in AR frequency. We discuss why differences in the quan-
320 titative definition of ARs may cause different behavior in future climate simulations and
321 its implications in Section 4. We have run the same analysis for seasonal averages for
322 all four seasons, and the seasonal climatology and seasonal trends are similar to the an-
323 nual average results presented in Figure 1.

324 We decompose the changes in AR frequency by changes in AR area A and AR count
325 N ; Figure 2b shows the median size of AR objects versus the median number of AR ob-
326 jects counted at any given time. In the historical simulations, the ARDTs appear to clus-
327 ter along a continuum, with ARDTs typically detecting 5–20 ARs, which is consistent
328 with manual counts of ARs in synoptic maps (Zhu & Newell, 1998; O’Brien, Risser, et
329 al., 2020). **Tempest** is a notable exception, with AR counts ranging from 20–50. In or-
330 der to aid in interpreting the continuum along which the ARDTs lay in Figure 2b, we
331 add lines of constant global area A_{\oplus} percentage (calculated as $100\% \cdot A \cdot N / A_{\oplus}$). These
332 show that algorithms typically detect ARs such that approximately 5% of the Earth’s
333 surface is covered in AR objects in the historical simulations. Therefore, we can inter-
334 pret the relative location of ARDTs in Figure 2b as an indicator of the relative spatial
335 coherence of AR objects: ARDTs on the left detect few, large AR objects and ARDTs
336 on the right detect many small AR objects. This grouping along lines of constant global

337 area fraction is an emergent collective behavior of the ARDTs, and we speculate that
338 it is associated with the tuning process for each algorithm. AR coherence might make
339 a useful measure for objective grouping of AR results in future ARTMIP studies.

340 Figure 2b shows that four of the ARDTs (except **Tempest** and **TECA-BARD v1.0.1**)
341 tend to detect more ARs and larger ARs in the future simulations. These changes re-
342 sult in increases in the global area coverage of AR objects: changing from $\sim 5\%$ global
343 area to $\sim 7\%$ global area. The global count of AR objects does not change in the **TECA-BARD v1.0.1**
344 algorithm, though there are slight increases in AR area in some simulations. In contrast,
345 the **Tempest** algorithm indicates increases in global AR count, with very little change
346 in AR area.

347 There is an indication that the resolution of the underlying model may affect the
348 characteristics of detected ARs for some ARDTs. The CMIP6 BCC-CSM2-MR, CMIP6
349 MRI-ESM2-0, and CMIP5 CCSM4 simulations—which are the three highest resolution
350 simulations analyzed (Table S1)—tend to occur on the right side of each ARDT cluster:
351 ARs in these simulations are systematically less coherent. However, the model resolu-
352 tion does not appear to affect the climate change signal evident in Figure 2b. Further,
353 the CMIP5/6 simulations analyzed here do not attempt to control for model resolution;
354 the CMIP6 HighResMIP experiment (Haarsma et al., 2016) could provide a way to ex-
355 amine resolution effects more systematically.

356 3.3 Sources of Uncertainty in End-of-Century Projections of ARs

357 The results in Figure 1 indicate that there may be substantial uncertainty in fu-
358 ture AR frequency associated with choice of ARDT. Further, it is not clear from the spa-
359 tial maps in Figure 1 whether the trends in AR frequency evident over the ocean (e.g.,
360 the decrease in the southeastern Atlantic) extend to the coastal areas where AR pres-
361 ence matters for western-coastal water cycles and hydrometeorological impacts. We quan-
362 tify these changes and their uncertainty in Figure 2c,d, which show the mean trend in
363 AR frequency for the Pacific (Figure 2c) and Atlantic west coasts (Figure 2d) from 1951-
364 2099. Figure 2c,d shows trends for all ARDTs listed in Table S1: both regional and global
365 ARDTs.

366 Figure 2c,d shows that coastal areas in both the Pacific and Atlantic show increas-
367 ing trends in AR frequency (+2–5 AR days per year per century in the midlatitudes),
368 and the full spread of the blue and light blue shading in Figure 2c,d shows the full range
369 of trends from all ARDTs and all models. There are two areas where **TECA-BARD v1.0.1**
370 indicates weakly decreasing trends (Figure S3 shows the trends by model and by algo-
371 rithm): southern Chile, near 40°S , and near the entrance of the Mediterranean Sea from
372 35°N to almost 60°N , which spans the Mediterranean, Iberian Peninsula and British Isles.
373 It is noteworthy that this decrease is compensated by an increase in AR frequency pole-
374 ward of these regions, indicating a poleward shift in the AR frequency. Otherwise all model-
375 ARDT combinations indicate increasing trends in landfalling AR frequency for both Pa-
376 cific and Atlantic ARs in both hemispheres.

377 Large uncertainty appears in the magnitude of the trends, which ranges from just
378 below 0 days/yr/century to over 15 days/year/century, depending on location. There
379 are two main components of uncertainty in these trends: uncertainty associated with choice
380 of model simulation, and uncertainty associated with choice of ARDT. We decompose
381 the uncertainty as $\sigma_T^2 \approx \sigma_A^2 + \sigma_M^2$, where σ_T^2 is the total variance, σ_A^2 is the variance
382 across ARDTs of each ARDT’s multi-model mean, and σ_M^2 is the variance across mod-
383 els for each model’s multi-ARDT mean. These variances can equivalently be viewed as
384 the variance down the rightmost column in Figure S3 (σ_M^2) and the variance across the
385 bottommost row in Figure S3 (σ_A^2), (excluding the multi-model/multi-ARDT mean in
386 the bottom right corner of Figure S3 and excluding trends from MERRA-2).

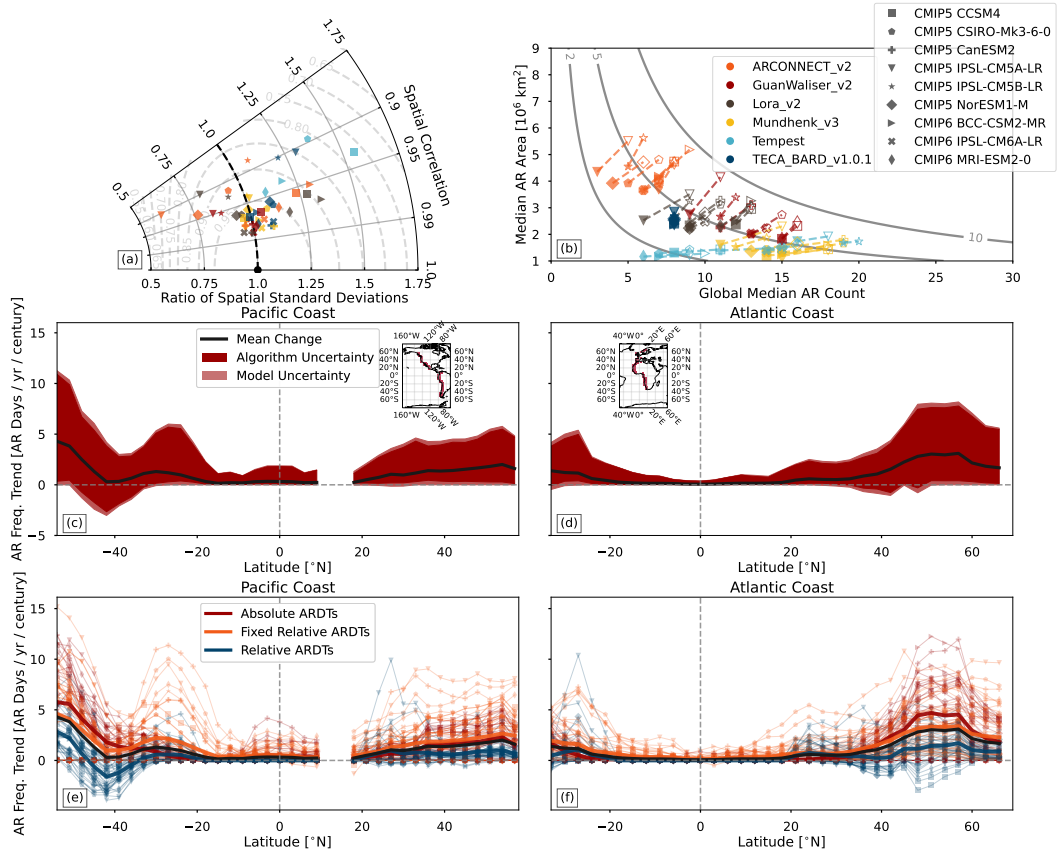


Figure 2. (a) A Taylor diagram comparing the spatial correlation (azimuthal axis) and spatial variability (radial axis) of AR frequency between CMIP5 and 6 simulations (denoted by different symbols) and the MERRA-2 reanalysis. Colors indicate different AR detection algorithms (legend in panel b). Gray dashed lines show lines of constant skill score (Taylor, 2001). (b) Median AR area vs global median AR count for all available combinations of ARDTs (marker colors) and simulations (marker symbols). Filled symbols indicate calculations performed on the 1981-2010 period of each simulation, and open symbols indicate calculations on the 2070-2099 period (two exceptions noted in Text S3). Gray contours show lines of constant fractional areal coverage of ARs (shown as a percentage of Earth’s area), calculated as the product of AR area and AR count, divided by Earth’s area. (c and d) Trends in AR frequency (black curve) and associated total range of uncertainty (blue and light blue shading) for the west-facing (c) Pacific coastline and (d) Atlantic coastline. Dark blue shading indicates the portion of uncertainty associated with AR detection and the light blue shading indicates the portion of the spread associated with models (across both CMIP5 and CMIP6). The area of dark blue shading is proportional to $\sigma_A^2/\sigma_T^2 \cdot (\max - \min)$, where ‘max’ and ‘min’ are the minimum and maximum trend at each latitude. (e and f) as in (c and d), but showing individual ARDT-model combinations. Markers indicate simulations (legend in panel b) and colors indicate the ARDT classification. Bold lines indicate the mean trend across the ARDT classification. The inset maps in (c) and (d) show the Pacific and Atlantic coast masks respectively.

387 This decomposition shows that uncertainty associated with choice of ARDT ac-
388 counts for most of the spread in the climate change signal across all latitudes in both
389 the Pacific and Atlantic coasts. In essence, uncertainty associated with the numerical
390 definition of ARs dominates the combined uncertainty associated with choice of model
391 and choice of model epoch (CMIP5 vs CMIP6). As shown in Figures 1 and 2, compar-
392 ison against reanalysis shows that most ARDT-model pairs perform well when compared
393 with reanalysis, so this measure of model skill does not provide a way to reduce the un-
394 certainty, since all ARDTs perform equivalently well on average. If there were a stan-
395 dard against which to rank ARDTs, it might be possible to utilize ARDT-weighting ap-
396 proaches to narrow the spread; but such a standard currently does not exist, and so such
397 a weighting approach is not possible.

398 The spread in the number of detected ARs accounts for some of the spread in trends.
399 If the trends in Figures 2c-f are normalized by the number of ARs detected, the rela-
400 tive magnitude of the ARDT-related uncertainty drops, though it is still large: above
401 50% of the total spread in the midlatitudes. (Note that this quantity is ill-defined in re-
402 gions, such as the tropics, where few or no ARs are detected.) As suggested by O'Brien,
403 Risser, et al. (2020), this suggests that constraining the total number of ARs is of cen-
404 tral importance to reducing uncertainty about AR variability and change.

405 4 Discussion and Conclusions

406 While there have been studies examining future changes in ARs (e.g., Payne et
407 al., 2020) and studies examining uncertainty related to choice of ARDT (e.g., Rutz et
408 al., 2019), no existing study has attempted to quantify the attribution of ARDT uncer-
409 tainty for climate change by evaluating model uncertainty versus ARDT uncertainty. The
410 ARTMIP Tier2 CMIP5/6 experiment provides a unique opportunity for such a study.
411 The results from this experiment show that most ARDTs project an increase in AR fre-
412 quency, with mean trends of approximately +2-5 AR days/year per century along the
413 western coastlines of North America, South America, Southern Africa, and Europe (Fig-
414 ure 2c,d). These changes are relatively large, given that the AR frequency in coastal re-
415 gions is typically between 10-20 AR days per year, though this depends strongly on ge-
416 ographic region and the ARDT used (Figure 1). However, there is considerable spread
417 in the magnitude, with some ARDT-model combinations indicating negative trends (south-
418 ern Chile and the European west coast from the Iberian Peninsula to the British Isles)
419 with a clear AR shift poleward and other ARDT-model combinations indicating posi-
420 tive trends of ARs in all regions with a magnitude up to ~ 15 AR days per century. Care
421 must be taken when making general statements about the sign of AR frequency/size/count
422 trends, since this work shows that the sign and magnitude of the trends are linked to choices
423 that ARDT designers make when translating the qualitative AMS definition into a quan-
424 titative definition. Specific statements can be made if one settles on a narrow quanti-
425 tative definition, as is typically done when seeking answers to questions about processes
426 or impacts related to ARs (e.g. orographic precipitation, ice sheet melt, or process drivers).

427 Globally, all ARDTs indicate either an increase in the total number of ARs, an in-
428 crease in the areal extent of ARs, or both (Figure 2b). In the historical simulations, the
429 AR area vs size relationship for all ARDTs approximately falls along a line of constant
430 global coverage, with ARDTs in the historical simulations detecting ARs that cover ap-
431 proximately 5% of the global area. This number is somewhat smaller than the 10% global
432 area indicated by Zhu and Newell (1998), which is likely because we are considering the
433 total global coverage, including the tropics, rather than the fraction of zonal circumfer-
434 ence in the midlatitudes. It is nevertheless qualitatively consistent in the sense that ar-
435 eas of anomalously high moisture transport occupy a small fraction of the global area.
436 The global areal coverage increases in the future simulations to some degree in all ARDT
437 algorithms, with most indicating a several percent increase in the areal extent of ARs
438 due to increases in both AR size and count.

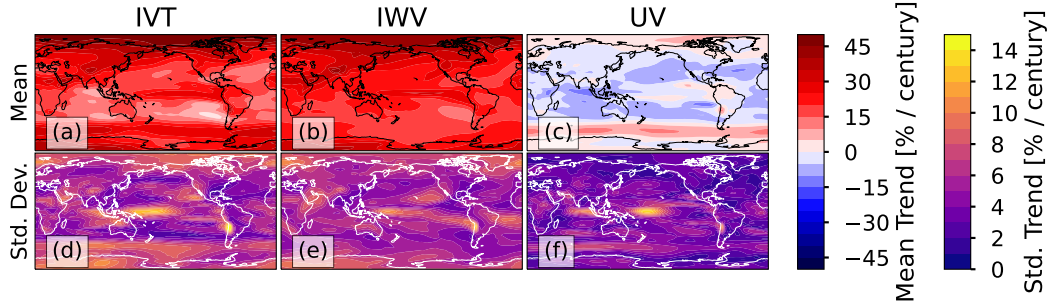


Figure 3. Trends in IVT, IWV, and $UV \equiv IVT/IWV$ among the CMIP5/6 models, calculated from approximately 1950–2100. Panels (a-c) show the mean trend, and panels (d-f) show the standard deviation of the trends. Trends for each model are shown in Figure S4.

439 These results further show that future changes in AR frequency can qualitatively
 440 differ depending on the type of ARDT used. We aggregate trends by AR classification
 441 (see Sections 2 and Text S2) in Figures 2e,f. This aggregation shows that use of any ab-
 442 solute thresholds (*absolute ARDTs*) and time-independent relative thresholds (*fixed rel-*
 443 *ative ARDTs*) tend to produce increases in AR frequency, whereas use of time-dependent
 444 relative thresholds (*relative ARDTs*) tend to produce patterns more indicative of a pole-
 445 ward shift. *Absolute ARDTs* and *fixed relative ARDTs*, with thresholds that do not change
 446 in time, would be expected to increase the frequency of exceedence of regions above the
 447 historical thresholds: more detected AR days in a warmer climate. Such ARDTs are de-
 448 signed to detect increases in occurrence of regions with high IVT, which are important
 449 for AR impacts. In contrast, *relative ARDTs* (e.g., TECA-BARD v1.0.1) are designed to
 450 only account for dynamical—rather than thermodynamical—changes in ARs.

451 To illustrate the thermodynamic and dynamic changes in IVT, Figures 3a–c shows
 452 the model-mean trend in IVT, IWV and the moisture-weighted wind $UV \equiv IVT/IWV$
 453 (it can readily be demonstrated that UV represents the vertically averaged wind, weighted
 454 by the specific humidity at each height). The model spread in these trends are shown
 455 in Figures 3d–f (Figure S4 shows the trends for each model). Both the IVT and IWV
 456 fields increase at a rate of 20–40% per century in the model simulations, whereas the UV
 457 field has much smaller changes: decreases in wind of 5–15%/century in most of the tropics
 458 and midlatitudes and increases of similar magnitude in the polar regions. Because
 459 IVT is the product of IWV and UV, the fractional trend in IVT can be decomposed into
 460 a sum of the fractional trends in each quantity:

$$\frac{1}{IVT} \frac{\partial IVT}{\partial t} = \frac{1}{IWV} \frac{\partial IWV}{\partial t} + \frac{1}{UV} \frac{\partial UV}{\partial t}.$$

461 The similarity of the IVT and IWV trend magnitudes implies that most of the trend in
 462 IVT is due to the thermodynamic component: the increase in atmospheric water vapor
 463 content due to Clausius-Clapeyron (CC) scaling. In contrast, the dynamic change is more
 464 indicative of a poleward shift in the magnitude of moisture-transporting winds. It is worth
 465 noting that the results presented in Figure 3 are independent of ARDT, though they do
 466 help explain some of the differences across ARDTs.

467 The literature documents two major modes of AR change associated with climate
 468 change: (1) a quasi-global increase in IVT associated with CC scaling (thermodynamic;
 469 Payne et al., 2020), and (2) a poleward shift in ARs (dynamic; Payne et al., 2020) as-
 470 sociated with the poleward shift in the midlatitude storm tracks (Chang et al., 2012).

471 Poleward shift patterns appear to co-exist to some extent with quasi-global increases in
472 AR frequency in some simulations (e.g., the CMIP5 CSIRO-MK3-6-0 simulation; see Fig-
473 ure S3) for all ARDTs. We argue that *absolute ARDTs* and *fixed relative ARDTs* are
474 more sensitive to thermodynamic changes than *relative ARDTs*. The strongest increase
475 in the *absolute* and *fixed relative ARDTs* compared to *relative ARDTs* explains the sen-
476 sitivity to ARDT choice especially approaching colder and drier polar regions. The fu-
477 ture, much stronger, increase in high latitude temperature associated with polar ampli-
478 fication, compared to other regions, together with hydrological cycle intensification will
479 be more evident in the *absolute* and *fixed relative ARDTs* compared to the *relative ARDTs*.

480 This categorization of ARDTs does not perfectly explain the spread in trends, as
481 *Tempest* and *TECA-BARD v1.0.1* trends in Figure 1 are qualitatively different; as such
482 the mean trends for the *relative ARDTs* in Figures 2e,f should be interpreted with cau-
483 tion. We hypothesize that they differ due to how the two methods identify relative peaks
484 in the IVT field: *Tempest* uses the Laplacian to find local ridges in the IVT field, whereas
485 the percentile-based approach in *TECA-BARD v1.0.1* seeks out the relatively highest IVT
486 locations in each timestep. It is possible that *Tempest* identifies relatively small, weak
487 ARs that *TECA-BARD v1.0.1* misses because they are weak enough to fall below its rel-
488 ative threshold. If this is the case, it could imply that the contrasting regions, where *Tempest*
489 shows an increase and *TECA-BARD v1.0.1* shows a decrease, are associated with an in-
490 crease in the occurrence of relatively weak ARs that *TECA-BARD v1.0.1* misses. This is
491 worth studying in a future paper.

492 It is worth noting here that trend patterns in the MERRA-2 reanalysis are sim-
493 ilar across ARDTs (Figure S3), with all ARDTs indicating a poleward shift in ARs. This
494 might suggest that the observed poleward shift in the storm tracks (Fyfe, 2003; Davis
495 & Rosenlof, 2012; Pena-Ortiz et al., 2013; Tilinina et al., 2013; Lucas et al., 2014; Man-
496 ney & Hegglin, 2018) dominates over quasi-global increases in IVT in the historical record.
497 This should be investigated further as part of the Tier 2 Reanalysis experiment.

498 The algorithm-wise validation of simulated ARs (Figure 2a) shows that models ex-
499 hibit spatial patterns of AR occurrence similar to those in reanalysis, as evidenced by
500 high Taylor skill scores for spatial correlations and standard deviations. This is a note-
501 worthy result in the context of the ARDT uncertainty shown here. If only one algorithm
502 is used in a study, such validation could give false confidence in the robustness of results.
503 It therefore seems important to explicitly include ARDT uncertainty as part of evalu-
504 ation of a model’s ability to represent ARs, which, relatedly, points to the utility of ap-
505 propriate ensemble weighting strategies to help reduce such uncertainty (e.g., Massoud
506 et al., 2019). It also highlights the value of AR-related, but not ARDT-dependent, eval-
507 uations of models (e.g., Payne & Magnusdottir, 2015).

508 Recent work involving manual identification of ARs by experts (Prabhat et al., 2020;
509 O’Brien, Risser, et al., 2020) suggests that the spread in AR algorithm behavior is linked
510 to differences in opinion about what does and does not constitute an AR. O’Brien, Risser,
511 et al. (2020) show that this spread in subjective opinion projects directly on to quan-
512 titative differences in the sign of the correlation coefficient between an El Niño index and
513 global AR count. Such differences in subjective opinion likely also play a role in the quan-
514 titative choices made by various ARDT designers. Gimeno et al. (2021) add some dis-
515 cussion concerning the diversity of the different meteorological patterns that can be as-
516 sociated with the qualitative definition of ARs, and there is no guarantee that all so-called
517 ARs are associated with the same meteorological patterns. Given this spread in expert
518 opinion, and given that there is no agreed-upon theoretical or numerical definition of what
519 defines an AR, there is presently no way to objectively assess whether one ARDT is bet-
520 ter than another.

521 Somewhat relatedly, the ARTMIP project has established that different AR detec-
522 tors are designed with different—and equally legitimate—purposes (Shields et al., 2018;

523 Rutz et al., 2019; Ralph, Wilson, et al., 2019). Some ARDTs intentionally choose to dis-
524 criminate ARs from the background based on absolute thresholds in IVT (e.g., Rutz et
525 al., 2014), since it is well-established that coastal orographic precipitation is directly linked
526 to IVT magnitude (Neiman et al., 2002; Ralph et al., 2004, 2005; Neiman, Ralph, Wick,
527 Kuo, et al., 2008; Ralph, Rutz, et al., 2019); such a design choice makes it easy to re-
528 late ARDT results directly to hydrometeorological impacts. Other algorithms (e.g., Shields
529 & Kiehl, 2016b; O’Brien, Risser, et al., 2020) intentionally use relative thresholds in order
530 to avoid increases in AR detection due to long-term increases in atmospheric water
531 vapor. Both are valid for the purposes for which they were designed: absolute methods
532 detect areas that will likely lead to hydrometeorological impacts—which will increase in
533 a warmer climate—and relative methods seek to focus on the core of regions associated
534 with anomalous vapor transport.

535 These results suggest that new projects investigating future changes in the statis-
536 tics and characteristics of ARs should explicitly consider ARDT uncertainty as a core
537 part of the experimental design. This study makes it clear that ARDT design choices
538 can have a major impact on the results of climate change studies, and with dozens of ARDTs
539 in use (Rutz et al., 2019), the uncertainty associated with their varying methods will not
540 be going away soon. Furthermore, using multiple ARDTs can be advantageous. For ex-
541 ample, will an increase in ARs and precipitation result primarily from an increase in IWV
542 or an increase in UV wind? Having ARDTs that weigh these variables differently can
543 help answer these questions. The Bayesian, multi-ARDT approach of O’Brien, Risser,
544 et al. (2020) can quantify parametric uncertainty associated with a single ARDT, but
545 it is not yet clear how parametric uncertainty compares to structural uncertainty (i.e.,
546 choices in what heuristic rules to employ in the ARDT). There are at least four ARDT
547 codes that are now in the public domain (Mundhenk_v1, Guan_Waliser_v2, Tempest, and
548 TECA-BARD v1.0.1; see [https://www.cgd.ucar.edu/projects/artmip/algorithms](https://www.cgd.ucar.edu/projects/artmip/algorithms.html)
549 [.html](https://www.cgd.ucar.edu/projects/artmip/algorithms.html) for a full list of ARDTs that have participated in ARTMIP), and we encourage
550 current and future ARDT designers to likewise enter their codes into the public domain
551 in order to facilitate such uncertainty exploration in future studies.

552 Ralph et al. (2018) provide a concise, qualitative definition of ARs, and this has
553 been a major benefit to the AR research community. They intentionally chose to “leave
554 specifications of how the boundaries of an AR are to be quantified open for future and
555 specialized developments.” The results in this manuscript demonstrate that the choice
556 of how to define AR boundaries—the fundamental job of an ARDT—have a demonstra-
557 bly large control on the statistics of ARs detected in future climate simulations. These
558 results suggest that the AR research community would further benefit from studies that
559 aim to quantitatively constrain the definition of ARs; e.g., with first-principles analy-
560 ses that constrain AR properties like size, count, etc. Such constraints could help reduce
561 uncertainty associated with ARDT design choice (and parameter choice), and by exten-
562 sion they could constrain results concerning ARs and future climate change. That said,
563 given that different experiments motivate different ARDT design choices (e.g., absolute
564 vs relative thresholds), it seems unavoidable that some of this uncertainty is irreducible.
565 It is clear, however, that it is imperative for studies to explore and understand the im-
566 plications of this uncertainty.

567 This study focuses on a bulk, global perspective of uncertainty associated with ARDTs
568 and simulations in the Tier 2 CMIP5/6 experiment. There are many other types of more
569 detailed analyses that others could take on. For example, this study has not considered
570 the temporal characteristics of ARs, since relatively few existing ARDTs track ARs as
571 they propagate in time; a recent study by Zhou et al. (2021) uses a common temporal
572 tracking algorithm on multiple ARDTs, and such an approach could be applied to the
573 Tier 2 dataset. We encourage others in the research community to utilize this dataset
574 for research on future ARs and climate change (see data availability statement in Ac-
575 knowledgements). In particular, it seems valuable to revisit past studies of ARs and fu-

576 ture climate change in the context of ARDT uncertainty. Payne et al. (2020) review the
577 numerous results concerning the future of ARs that have appeared in the literature in
578 the last decade. There are almost as many ARDTs as there are such results, which makes
579 intercomparison of the results challenging. The Tier 2 CMIP5/6 dataset provides a way
580 to revisit many—if not all—of these previous results within a uniform experimental frame-
581 work.

582 Prior to ARTMIP, it was assumed that the various ARDTs in the literature were
583 simply different methods of looking at the same dynamical phenomenon. Recent papers
584 associated with ARTMIP show that that is true for strong ARs (with high IVT, e.g., Rutz
585 et al., 2019; Lora et al., 2020), but that there is disagreement among the various ARDTs
586 for weaker ARs. Further, Zhang et al. (2019) show that approximately 20% of ARs are
587 not associated with a nearby extratropical cyclone (under their ARDT criteria), suggest-
588 ing that this subset of ARs may have a different dynamical origin. This raises some ques-
589 tions that remain unanswered. *Are some ARDTs simply missing ARs that other ARDTs*
590 *are identifying, or is there more than one type of dynamical phenomenon that produces*
591 *AR-like objects; are some ARDTs more sensitive to one dynamical phenomenon and oth-*
592 *ers are more sensitive to another; and if there are multiple dynamical causes of ARs, do*
593 *they have different spatiotemporal responses to climate change?* These questions are likely
594 answerable with the datasets that have been produced by the ARTMIP project.

595 In summary, this initial analysis of the Tier 2 CMIP5/6 experiment shows that most
596 ARDTs and simulations indicate an increasing trend in AR frequency, size, and num-
597 ber in future simulations with strong radiative forcing. It also shows the critical impor-
598 tance of understanding the implications of uncertainty for AR-related research. Finally,
599 this paper introduces the publicly-available Tier 2 CMIP5/6 dataset, which may be a
600 valuable resource for answering fundamental questions about ARs and about ARs and
601 climate change.

602 Acknowledgments

603 The authors thank the multiple reviewers and editors whose feedback and commen-
604 tary greatly improved the quality and presentation of this manuscript.

605 This research was supported by the Director, Office of Science, Office of Biologi-
606 cal and Environmental Research of the U.S. Department of Energy Regional and Global
607 Climate Modeling Program (RGMA) and used resources of the National Energy Research
608 Scientific Computing Center (NERSC), also supported by the Office of Science of the
609 U.S. Department of Energy under Contract No. DE-AC02-05CH11231.

610 The contributions of T.A. O’Brien were supported in part by the U.S. Department
611 of Energy, Office of Science, Office of Biological and Environmental Research, Climate
612 and Environmental Sciences Division, Regional & Global Model Analysis Program, un-
613 der Award Number DE-AC02-05CH11231; in part by the Environmental Resilience In-
614 stitute, funded by Indiana University’s Prepared for Environmental Change Grand Chal-
615 lenge initiative and in part by Lilly Endowment, Inc., through its support for the Indi-
616 ana University Pervasive Technology Institute. Alexandre M. Ramos is supported by the
617 Fundação para a Ciência e Tecnologia (FCT, Portugal) project “Weather Extremes in
618 the Euro Atlantic Region: Assessment and Impacts-WEx-Atlantic” (PTDC/CTA-MET/29233/2017).
619 Alexandre M. Ramos also acknowledges the Scientific Employment Stimulus 2017 from
620 FCT (CEECIND/00027/2017). Irina V. Gorodetskaya thanks FCT/MCTES for the fi-
621 nancial support to CESAM (UIDP/500017/2020+UIDB/500017/2020), through national
622 funds, and FCT Project ATLACE (CIRCNA/CAC/0273/2019). Eric J. Shearer is sup-
623 ported by the Ridge to Reef Graduate Training Program funded by NSF-NRT award DGE-
624 1735040.

625 We acknowledge the World Climate Research Programme, which, through its Work-
626 ing Group on Coupled Modelling, coordinated and promoted CMIP6. We thank the cli-
627 mate modeling groups for producing and making available their model output, the Earth
628 System Grid Federation (ESGF) for archiving the data and providing access, and the
629 multiple funding agencies who support CMIP6 and ESGF. We thank DOE’s RGMA pro-
630 gram area, the Data Management program, and NERSC for making this coordinated CMIP6
631 analysis activity possible.

632 ARTMIP is a grass-roots community effort and includes a collection of international
633 researchers from universities, laboratories, and agencies. Details on catalogues develop-
634 ers can be found on the ARTMIP website. ARTMIP has received support from the US
635 Department of Energy Office of Science Biological and Environmental Research (BER)
636 as part of the Regional and Global Model Analysis program, and the Center for West-
637 ern Weather and Water Extremes (CW3E) at Scripps Institute for Oceanography at the
638 University of California, San Diego.

639 ARTMIP Tier 2 CMIP5/6 catalogues can be found on the Climate Data Gateway:
640 doi.org/10.26024/s4p7-pf13 (<https://go.iu.edu/3ci2>)

641 References

- 642 Bao, J. W., Michelson, S. A., Neiman, P. J., Ralph, F. M., & Wilczak, J. M. (2006).
643 Interpretation of enhanced integrated water vapor bands associated with ex-
644 tratropical cyclones: Their formation and connection to tropical moisture.
645 *Monthly Weather Review*, *134*(4), 1063–1080. doi: 10.1175/MWR3123.1
- 646 Blamey, R. C., Ramos, A. M., Trigo, R. M., Tomé, R., & Reason, C. J. (2018).
647 The influence of atmospheric rivers over the South Atlantic on winter rain-
648 fall in South Africa. *Journal of Hydrometeorology*, *19*(1), 127–142. doi:
649 10.1175/JHM-D-17-0111.1
- 650 Boucher, O., Denvil, S., Caubel, A., & Foujols, M. A. (2019). *IPSL IPSL-CM6A-LR*
651 *model output prepared for CMIP6 ScenarioMIP ssp585*. Earth System Grid
652 Federation. Retrieved from <https://doi.org/10.22033/ESGF/CMIP6.5271>
653 (Version 20180803) doi: 10.22033/ESGF/CMIP6.5271
- 654 Browning, K. A., & Pardoe, C. W. (1973). Structure of low-level jet streams ahead
655 of mid-latitude cold fronts. *Quarterly Journal of the Royal Meteorological Soci-*
656 *ety*, *99*(422), 619–638. doi: 10.1002/qj.49709942204
- 657 Chang, E. K., Guo, Y., & Xia, X. (2012). CMIP5 multimodel ensemble projection of
658 storm track change under global warming. *Journal of Geophysical Research At-*
659 *mospheres*, *117*(23), 1–19. doi: 10.1029/2012JD018578
- 660 Davis, S. M., & Rosenlof, K. H. (2012, feb). A Multidiagnostic Intercom-
661 parison of Tropical-Width Time Series Using Reanalyses and Satellite
662 Observations. *Journal of Climate*, *25*(4), 1061–1078. Retrieved from
663 <http://journals.ametsoc.org/doi/10.1175/JCLI-D-11-00127.1> doi:
664 10.1175/JCLI-D-11-00127.1
- 665 Dettinger, M. D., Ralph, F. M., Das, T., Neiman, P. J., & Cayan, D. R. (2011). At-
666 mospheric Rivers, Floods and the Water Resources of California. *Water*, *3*(2),
667 445–478. doi: 10.3390/w3020445
- 668 Espinoza, V., Waliser, D. E., Guan, B., Lavers, D. A., & Ralph, F. M. (2018, may).
669 Global Analysis of Climate Change Projection Effects on Atmospheric Rivers.
670 *Geophysical Research Letters*, *45*(9), 4299–4308. Retrieved from [http://](http://doi.wiley.com/10.1029/2017GL076968)
671 doi.wiley.com/10.1029/2017GL076968 doi: 10.1029/2017GL076968
- 672 Eyring, V., Bony, S., Meehl, G. A., Senior, C. A., Stevens, B., Stouffer, R. J., &
673 Taylor, K. E. (2016, may). Overview of the Coupled Model Intercompari-
674 son Project Phase 6 (CMIP6) experimental design and organization. *Geo-*
675 *scientific Model Development*, *9*(5), 1937–1958. Retrieved from [https://](https://www.geosci-model-dev.net/9/1937/2016/)
676 www.geosci-model-dev.net/9/1937/2016/ doi: 10.5194/gmd-9-1937-2016

- 677 Fyfe, J. C. (2003). Extratropical Southern Hemisphere cyclones: Harbingers of
678 climate change? *Journal of Climate*, *16*(17), 2802–2805. doi: 10.1175/1520-
679 -0442(2003)016<2802:ESHCHO>2.0.CO;2
- 680 Gao, Y., Lu, J., & Leung, L. R. (2016, 09). Uncertainties in Projecting Future
681 Changes in Atmospheric Rivers and Their Impacts on Heavy Precipitation over
682 Europe. *Journal of Climate*, *29*(18), 6711–6726. Retrieved from <https://doi.org/10.1175/JCLI-D-16-0088.1> doi: 10.1175/JCLI-D-16-0088.1
- 683
684 Gao, Y., Lu, J., Leung, L. R., Yang, Q., Hagos, S., & Qian, Y. (2015a). Dynamical
685 and thermodynamical modulations on future changes of landfalling atmo-
686 spheric rivers over western north america. *Geophysical Research Letters*,
687 *42*(17), 7179–7186. Retrieved from <https://agupubs.onlinelibrary.wiley.com/doi/abs/10.1002/2015GL065435> doi: 10.1002/2015GL065435
- 688
689 Gao, Y., Lu, J., Leung, L. R., Yang, Q., Hagos, S., & Qian, Y. (2015b, sep). Dy-
690 namical and thermodynamical modulations on future changes of landfalling
691 atmospheric rivers over western North America. *Geophysical Research Let-
692 ters*, *42*(17), 7179–7186. Retrieved from <http://doi.wiley.com/10.1002/2015GL065435> doi: 10.1002/2015GL065435
- 693
694 Gelaro, R., McCarty, W., Suárez, M. J., Todling, R., Molod, A., Takacs, L., ...
695 Zhao, B. (2017, jul). The Modern-Era Retrospective Analysis for Research
696 and Applications, Version 2 (MERRA-2). *Journal of Climate*, *30*(14),
697 5419–5454. Retrieved from <http://journals.ametsoc.org/doi/10.1175/JCLI-D-16-0758.1> doi: 10.1175/JCLI-D-16-0758.1
- 698
699 Gershunov, A., Shulgina, T., Clemesha, R. E. S., Guirguis, K., Pierce, D. W., Det-
700 tinger, M. D., ... Ralph, F. M. (2019, dec). Precipitation regime change
701 in Western North America: The role of Atmospheric Rivers. *Scientific Re-
702 ports*, *9*(1), 9944. Retrieved from <http://www.nature.com/articles/s41598-019-46169-w> doi: 10.1038/s41598-019-46169-w
- 703
704 Gershunov, A., Shulgina, T., Ralph, F. M., Lavers, D. A., & Rutz, J. J. (2017,
705 aug). Assessing the climate-scale variability of atmospheric rivers affect-
706 ing western North America. *Geophysical Research Letters*, *44*(15), 7900–
707 7908. Retrieved from <http://doi.wiley.com/10.1002/2017GL074175> doi:
708 10.1002/2017GL074175
- 709
710 Gimeno, L., Algarra, I., Eiras-Barca, J., Ramos, A. M., & Nieto, R. (2021). Atmo-
711 spheric river, a term encompassing different meteorological patterns. *WIREs
Water*(December 2020), 1–14. doi: 10.1002/wat2.1558
- 712
713 Gimeno, L., Dominguez, F., Nieto, R., Trigo, R., Drumond, A., Reason, C. J., ...
714 Marengo, J. (2016). Major Mechanisms of Atmospheric Moisture Transport
715 and Their Role in Extreme Precipitation Events. *Annual Review of Environ-
716 -ment and Resources*, *41*(1), 117–141. doi: 10.1146/annurev-environ-110615-085558
- 717
718 Gorodetskaya, I. V., Tsukernik, M., Claes, K., Ralph, M. F., Neff, W. D., & Van
719 Lipzig, N. P. M. (2014, sep). The role of atmospheric rivers in anomalous
720 snow accumulation in East Antarctica. *Geophysical Research Letters*, *41*(17),
721 6199–6206. Retrieved from <http://doi.wiley.com/10.1002/2014GL060881>
doi: 10.1002/2014GL060881
- 722
723 Guan, B., Molotch, N. P., Waliser, D. E., Fetzer, E. J., & Neiman, P. J. (2010,
724 oct). Extreme snowfall events linked to atmospheric rivers and surface air
725 temperature via satellite measurements. *Geophysical Research Letters*, *37*(20),
726 n/a–n/a. Retrieved from <http://doi.wiley.com/10.1029/2010GL044696>
doi: 10.1029/2010GL044696
- 727
728 Guan, B., & Waliser, D. E. (2015, dec). Detection of atmospheric rivers: Evalu-
729 ation and application of an algorithm for global studies. *Journal of Geophysi-
730 cal Research: Atmospheres*, *120*(24), 12514–12535. Retrieved from <http://doi.wiley.com/10.1002/2015JD024257> doi: 10.1002/2015JD024257
- 731
732 Guan, B., & Waliser, D. E. (2017). Atmospheric rivers in 20 year weather and cli-

- 732 mate simulations: A multimodel, global evaluation. *Journal of Geophysical Re-*
733 *search*, 122(11), 5556–5581. doi: 10.1002/2016JD026174
- 734 Guan, B., Waliser, D. E., & Ralph, F. M. (2018, 02). An Intercomparison between
735 Reanalysis and Dropsonde Observations of the Total Water Vapor Transport
736 in Individual Atmospheric Rivers. *Journal of Hydrometeorology*, 19(2), 321-
737 337. Retrieved from <https://doi.org/10.1175/JHM-D-17-0114.1> doi:
738 10.1175/JHM-D-17-0114.1
- 739 Haarsma, R. J., Roberts, M. J., Vidale, P. L., Senior, C. A., Bellucci, A., Bao, Q.,
740 ... von Storch, J.-S. (2016, nov). High Resolution Model Intercomparison
741 Project (HighResMIP v1.0) for CMIP6. *Geoscientific Model Development*,
742 9(11), 4185–4208. Retrieved from [http://www.geosci-model-dev.net/9/
743 4185/2016/https://gmd.copernicus.org/articles/9/4185/2016/](http://www.geosci-model-dev.net/9/4185/2016/https://gmd.copernicus.org/articles/9/4185/2016/) doi:
744 10.5194/gmd-9-4185-2016
- 745 Hagos, S., Ruby Leung, L., Yang, Q., Zhao, C., & Lu, J. (2015). Resolu-
746 tion and dynamical core dependence of atmospheric river frequency in
747 global model simulations. *Journal of Climate*, 28(7), 2764–2776. doi:
748 10.1175/JCLI-D-14-00567.1
- 749 Huang, H., Patricola, C. M., Bercos-Hickey, E., Zhou, Y., Rhoades, A., Risser,
750 M. D., & Collins, W. D. (2021). Sources of subseasonal-to-seasonal predictabil-
751 ity of atmospheric rivers and precipitation in the western United States.
752 *Journal of Geophysical Research: Atmospheres*, 126, e2020JD034053. doi:
753 10.1029/2020JD034053
- 754 Huning, L. S., Margulis, S. A., Guan, B., Waliser, D. E., & Neiman, P. J. (2017).
755 Implications of Detection Methods on Characterizing Atmospheric River Con-
756 tribution to Seasonal Snowfall Across Sierra Nevada, USA. *Geophysical Re-*
757 *search Letters*, 44(20), 10,445–10,453. doi: 10.1002/2017GL075201
- 758 Iskenderian, H. (1995, jun). A 10-Year Climatology of Northern Hemisphere
759 Tropical Cloud Plumes and Their Composite Flow Patterns. *Journal of Cli-*
760 *mate*, 8(6), 1630–1637. Retrieved from [http://journals.ametsoc.org/
761 doi/10.1175/1520-0442\(1995\)008%3C1630:AYCONH%3E2.0.CO;2](http://journals.ametsoc.org/doi/10.1175/1520-0442(1995)008%3C1630:AYCONH%3E2.0.CO;2) doi:
762 10.1175/1520-0442(1995)008<1630:AYCONH>2.0.CO;2
- 763 Kiehl, J. T., Shields, C. A., Snyder, M. A., Zachos, J. C., & Rothstein, M. (2018).
764 Greenhouse- and orbital-forced climate extremes during the early Eocene.
765 *Philosophical Transactions of the Royal Society A: Mathematical, Physical and*
766 *Engineering Sciences*, 376(2130). doi: 10.1098/rsta.2017.0085
- 767 Kiladis, G. N., & Weickmann, K. M. (1992, sep). Extratropical Forcing of Trop-
768 ical Pacific Convection during Northern Winter. *Monthly Weather Re-*
769 *view*, 120(9), 1924–1939. Retrieved from [http://journals.ametsoc.org/
770 doi/10.1175/1520-0493\(1992\)120%3C1924:EFOTPC%3E2.0.CO;2](http://journals.ametsoc.org/doi/10.1175/1520-0493(1992)120%3C1924:EFOTPC%3E2.0.CO;2) doi:
771 10.1175/1520-0493(1992)120<1924:EFOTPC>2.0.CO;2
- 772 Kuhnel, I. (1989, sep). Tropical-extratropical cloudband climatology based on satel-
773 lite data. *International Journal of Climatology*, 9(5), 441–463. Retrieved from
774 <https://onlinelibrary.wiley.com/doi/10.1002/joc.3370090502> doi: 10
775 .1002/joc.3370090502
- 776 Lackmann, G. M., & Gyakum, J. R. (1999). Heavy cold-season precipitation in
777 the northwestern United States: Synoptic climatology and an analysis of the
778 flood of 17-18 January 1986. *Weather and Forecasting*, 14(5), 687–700. doi:
779 10.1175/1520-0434(1999)014<0687:HCSPIT>2.0.CO;2
- 780 Lau, K.-M., & Chan, P. H. (1988, feb). Intraseasonal and Interannual Variations of
781 Tropical Convection: A Possible Link between the 40–50 Day Oscillation and
782 ENSO? *Journal of the Atmospheric Sciences*, 45(3), 506–521. Retrieved from
783 [http://journals.ametsoc.org/doi/10.1175/1520-0469\(1988\)045%3C0506:
784 IAIVOT%3E2.0.CO;2](http://journals.ametsoc.org/doi/10.1175/1520-0469(1988)045%3C0506:IAIVOT%3E2.0.CO;2) doi: 10.1175/1520-0469(1988)045<0506:IAIVOT>2.0.CO;
785 2
- 786 Lavers, D. A., Pappenberger, F., Richardson, D. S., & Zsoter, E. (2016). ECMWF

- 787 Extreme Forecast Index for water vapor transport: A forecast tool for atmo-
788 spheric rivers and extreme precipitation. *Geophysical Research Letters*, 43(22),
789 11,852–11,858. doi: 10.1002/2016GL071320
- 790 Lavers, D. A., Ralph, F. M., Waliser, D. E., Gershunov, A., & Dettinger, M. D.
791 (2015, jul). Climate change intensification of horizontal water vapor
792 transport in CMIP5. *Geophysical Research Letters*, 42(13), 5617–5625.
793 Retrieved from <http://doi.wiley.com/10.1002/2015GL064672> doi:
794 10.1002/2015GL064672
- 795 Lavers, D. A., & Villarini, G. (2013). The nexus between atmospheric rivers and ex-
796 treme precipitation across Europe. *Geophysical Research Letters*, 40(12), 3259–
797 3264. doi: 10.1002/grl.50636
- 798 Lavers, D. A., Villarini, G., Allan, R. P., Wood, E. F., & Wade, A. J. (2012, oct).
799 The detection of atmospheric rivers in atmospheric reanalyses and their links
800 to British winter floods and the large-scale climatic circulation. *Journal of*
801 *Geophysical Research Atmospheres*, 117(20), 1–13. Retrieved from [http://](http://doi.wiley.com/10.1029/2012JD018027)
802 doi.wiley.com/10.1029/2012JD018027 doi: 10.1029/2012JD018027
- 803 Lavers, D. A., Waliser, D. E., Ralph, F. M., & Dettinger, M. D. (2016). Pre-
804 dictability of horizontal water vapor transport relative to precipitation: En-
805 hancing situational awareness for forecasting western U.S. extreme precipi-
806 tation and flooding. *Geophysical Research Letters*, 43(5), 2275–2282. doi:
807 10.1002/2016GL067765
- 808 Leung, L.-R., & Qian, Y. (2009). Atmospheric rivers induced heavy precipita-
809 tion and flooding in the western U.S. simulated by the WRF regional climate
810 model. *Geophysical Research Letters*, 36(3), 1–6. doi: 10.1029/2008GL036445
- 811 Lora, J. M., Mitchell, J. L., Risi, C., & Tripathi, A. E. (2017, jan). North Pacific
812 atmospheric rivers and their influence on western North America at the Last
813 Glacial Maximum. *Geophysical Research Letters*, 44(2), 1051–1059. Re-
814 trieved from <http://doi.wiley.com/10.1002/2016GL071541>[https://](https://onlinelibrary.wiley.com/doi/abs/10.1002/2016GL071541)
815 onlinelibrary.wiley.com/doi/abs/10.1002/2016GL071541 doi:
816 10.1002/2016GL071541
- 817 Lora, J. M., Shields, C. A., & Rutz, J. J. (2020, oct). Consensus and Disagreement
818 in Atmospheric River Detection: ARTMIP Global Catalogues. *Geophysical Re-*
819 *search Letters*, 47(20), 1–10. Retrieved from [https://onlinelibrary.wiley](https://onlinelibrary.wiley.com/doi/10.1029/2020GL089302)
820 [.com/doi/10.1029/2020GL089302](https://onlinelibrary.wiley.com/doi/10.1029/2020GL089302) doi: 10.1029/2020GL089302
- 821 Lucas, C., Timbal, B., & Nguyen, H. (2014, jan). The expanding tropics: a crit-
822 ical assessment of the observational and modeling studies. *WIREs Climate*
823 *Change*, 5(1), 89–112. Retrieved from [https://onlinelibrary.wiley.com/](https://onlinelibrary.wiley.com/doi/10.1002/wcc.251)
824 [doi/10.1002/wcc.251](https://onlinelibrary.wiley.com/doi/10.1002/wcc.251) doi: 10.1002/wcc.251
- 825 Manney, G. L., & Hegglin, M. I. (2018). Seasonal and regional variations of long-
826 term changes in upper-tropospheric jets from reanalyses. *Journal of Climate*,
827 31(1), 423–448. doi: 10.1175/JCLI-D-17-0303.1
- 828 Massoud, E., Espinoza, V., Guan, B., & Waliser, D. (2019). Global climate model
829 ensemble approaches for future projections of atmospheric rivers. *Earth's Fu-*
830 *ture*, 7(10), 1136–1151. Retrieved from [https://agupubs.onlinelibrary](https://agupubs.onlinelibrary.wiley.com/doi/abs/10.1029/2019EF001249)
831 [.wiley.com/doi/abs/10.1029/2019EF001249](https://agupubs.onlinelibrary.wiley.com/doi/abs/10.1029/2019EF001249) doi: 10.1029/2019EF001249
- 832 Mattingly, K. S., Mote, T. L., Fettweis, X., van As, D., Tricht, K. V., Lhermitte, S.,
833 ... Fausto, R. S. (2020). Strong summer atmospheric rivers trigger green-
834 land ice sheet melt through spatially varying surface energy balance and cloud
835 regimes. *Journal of Climate*, 33(16), 6809 - 6832. Retrieved from [https://](https://journals.ametsoc.org/view/journals/clim/33/16/jcliD190835.xml)
836 journals.ametsoc.org/view/journals/clim/33/16/jcliD190835.xml doi:
837 10.1175/JCLI-D-19-0835.1
- 838 McClenny, E. E., Ullrich, P. A., & Grotjahn, R. (2020, nov). Sensitivity of Atmo-
839 spheric River Vapor Transport and Precipitation to Uniform Sea Surface Tem-
840 perature Increases. *Journal of Geophysical Research: Atmospheres*, 125(21),
841 1–20. Retrieved from <https://onlinelibrary.wiley.com/doi/10.1029/>

- 2020JD033421 doi: 10.1029/2020JD033421
- 842
843 McGurk, J. P., Thompson, A. H., & Smith, N. R. (1987, apr). Moisture bursts
844 over the tropical Pacific Ocean. *Monthly Weather Review*, 115(4), 787–798.
845 Retrieved from [http://journals.ametsoc.org/doi/abs/10.1175/1520-](http://journals.ametsoc.org/doi/abs/10.1175/1520-0493(1987)115<0787:MBOTTP>2.0.CO;2)
846 [0493\(1987\)115<0787:MBOTTP>2.0.CO;2](http://journals.ametsoc.org/doi/abs/10.1175/1520-0493(1987)115<0787:MBOTTP>2.0.CO;2)
847 doi: 10.1175/1520-0493(1987)115<0787:MBOTTP>2.0.CO;2
- 848 Menemenlis, S., Lora, J. M., Lofverstrom, M., & Chandan, D. (2021). Influence of
849 stationary waves on mid-Pliocene atmospheric rivers and hydroclimate. *Global*
850 *and Planetary Change*, 204(May), 103557. Retrieved from [https://doi.org/](https://doi.org/10.1016/j.gloplacha.2021.103557)
851 [10.1016/j.gloplacha.2021.103557](https://doi.org/10.1016/j.gloplacha.2021.103557) doi: 10.1016/j.gloplacha.2021.103557
- 852 Mundhenk, B. D., Barnes, E. A., & Maloney, E. D. (2016). All-season climatology
853 and variability of atmospheric river frequencies over the North Pacific. *Journal*
854 *of Climate*, 29(13), 4885–4903. doi: 10.1175/JCLI-D-15-0655.1
- 855 Neiman, P. J., Ralph, F. M., White, A. B., Kingsmill, D. E., & Persson, P. O.
856 (2002). The statistical relationship between upslope flow and rainfall in
857 California’s coastal mountains: Observations during CALJET. *Monthly*
858 *Weather Review*, 130(6), 1468–1492. doi: 10.1175/1520-0493(2002)130<1468:
859 *TSRBUF>2.0.CO;2*
- 860 Neiman, P. J., Ralph, F. M., Wick, G. A., Kuo, Y. H., Wee, T. K., Ma, Z., ... Det-
861 tinger, M. D. (2008). Diagnosis of an intense atmospheric river impacting
862 the pacific northwest: Storm summary and offshore vertical structure observed
863 with COSMIC satellite retrievals. *Monthly Weather Review*, 136(11), 4398–
864 4420. doi: 10.1175/2008MWR2550.1
- 865 Neiman, P. J., Ralph, F. M., Wick, G. A., Lundquist, J. D., & Dettinger, M. D.
866 (2008). Meteorological characteristics and overland precipitation impacts of
867 atmospheric rivers affecting the West coast of North America based on eight
868 years of SSM/I satellite observations. *Journal of Hydrometeorology*, 9(1),
869 22–47. doi: 10.1175/2007JHM855.1
- 870 Neiman, P. J., Ralph, M. F., Moore, B. J., Hughes, M., Mahoney, K. M., Cordeira,
871 J. M., & Dettinger, M. D. (2013). The landfall and inland penetration of a
872 flood-producing atmospheric river in Arizona. Part I: Observed synoptic-scale,
873 orographic, and hydrometeorological characteristics. *Journal of Hydrometeorol-*
874 *ogy*, 14(2), 460–484. doi: 10.1175/JHM-D-12-0101.1
- 875 Newell, R. E., Newell, N. E., Zhu, Y., & Scott, C. (1992, dec). Tropospheric rivers?
876 - A pilot study. *Geophysical Research Letters*, 19(24), 2401–2404. Retrieved
877 from <http://doi.wiley.com/10.1029/92GL02916> doi: 10.1029/92GL02916
- 878 Newell, R. E., & Zhu, Y. (1994, jan). Tropospheric rivers: A one-year record and a
879 possible application to ice core data. *Geophysical Research Letters*, 21(2), 113–
880 116. Retrieved from <http://doi.wiley.com/10.1029/93GL03113> doi: 10.
881 1029/93GL03113
- 882 Newman, M., Kiladis, G. N., Weickmann, K. M., Ralph, M. F., & Sardeshmukh,
883 P. D. (2012). Relative contributions of synoptic and low-frequency ed-
884 dies to time-mean atmospheric moisture transport, including the role of at-
885 mospheric rivers. *Journal of Climate*, 25(21), 7341–7361. doi: 10.1175/
886 JCLI-D-11-00665.1
- 887 O’Brien, T. A., Payne, A. E., Shields, C. A., Rutz, J., Brands, S., Castellano,
888 C., ... Zhou, Y. (2020, jun). Detection Uncertainty Matters for Un-
889 derstanding Atmospheric Rivers. *Bulletin of the American Meteorolog-*
890 *ical Society*, 101(6), E790–E796. Retrieved from [https://doi.org/](https://doi.org/10.31223/osf.io/ftwgm)
891 [10.31223/osf.io/ftwgm](https://doi.org/10.31223/osf.io/ftwgm)[http://journals.ametsoc.org/doi/10.1175/](http://journals.ametsoc.org/doi/10.1175/BAMS-D-19-0348.1)
892 [BAMS-D-19-0348.1](http://journals.ametsoc.org/doi/10.1175/BAMS-D-19-0348.1)[https://journals.ametsoc.org/bams/article/101/6/](https://journals.ametsoc.org/bams/article/101/6/E790/345615/Detection-Uncertainty-Matters-for-Understanding)
893 [E790/345615/Detection-Uncertainty-Matters-for-Understanding](https://journals.ametsoc.org/bams/article/101/6/E790/345615/Detection-Uncertainty-Matters-for-Understanding) doi:
894 10.1175/BAMS-D-19-0348.1
- 895 O’Brien, T. A., Risser, M. D., Loring, B., Elbashandy, A. A., Krishnan, H., Johnson,
896 J., ... Collins, W. D. (2020, dec). Detection of atmospheric rivers with inline

- uncertainty quantification: TECA-BARD v1.0.1. *Geoscientific Model Development*, 13(12), 6131–6148. Retrieved from <https://www.geosci-model-dev-discuss.net/gmd-2020-55/#discussionhttps://gmd.copernicus.org/articles/13/6131/2020/> doi: 10.5194/gmd-13-6131-2020
- O'Neill, B. C., Tebaldi, C., Van Vuuren, D. P., Eyring, V., Friedlingstein, P., Hurtt, G., ... Sanderson, B. M. (2016). The Scenario Model Intercomparison Project (ScenarioMIP) for CMIP6. *Geoscientific Model Development*, 9(9), 3461–3482. doi: 10.5194/gmd-9-3461-2016
- Payne, A. E., Demory, M.-E., Leung, L. R., Ramos, A. M., Shields, C. A., Rutz, J. J., ... Ralph, F. M. (2020, mar). Responses and impacts of atmospheric rivers to climate change. *Nature Reviews Earth & Environment*, 1(3), 143–157. Retrieved from <http://dx.doi.org/10.1038/s43017-020-0030-5> doi: 10.1038/s43017-020-0030-5
- Payne, A. E., & Magnusdottir, G. (2015, nov). An evaluation of atmospheric rivers over the North Pacific in CMIP5 and their response to warming under RCP 8.5. *Journal of Geophysical Research: Atmospheres*, 120(21), 11,173–11,190. Retrieved from <http://doi.wiley.com/10.1002/2015JD023586> doi: 10.1002/2015JD023586
- Pena-Ortiz, C., Gallego, D., Ribera, P., Ordonez, P., & Alvarez-Castro, M. D. C. (2013, apr). Observed trends in the global jet stream characteristics during the second half of the 20th century. *Journal of Geophysical Research: Atmospheres*, 118(7), 2702–2713. Retrieved from <http://doi.wiley.com/10.1002/jgrd.50305> doi: 10.1002/jgrd.50305
- Polade, S. D., Gershunov, A., Cayan, D. R., Dettinger, M. D., & Pierce, D. W. (2017, dec). Precipitation in a warming world: Assessing projected hydroclimate changes in California and other Mediterranean climate regions. *Scientific Reports*, 7(1), 10783. Retrieved from <http://dx.doi.org/10.1038/s41598-017-11285-y> doi: 10.1038/s41598-017-11285-y
- Prabhat, P., Kashinath, K., Mudigonda, M., Kim, S., Kapp-Schwoerer, L., Graubner, A., ... Collins, W. (2020). ClimateNet: an expert-labelled open dataset and Deep Learning architecture for enabling high-precision analyses of extreme weather. *Geoscientific Model Development Discussions, In Review*(April). Retrieved from https://doi.org/10.5194/gmd-2020-72?utm{_}source=researcher{_}app{\&}utm{_}medium=referral{\&}utm{_}campaign=RESR{_}MRKT{_}Researcher{_}inbound doi: 10.5194/gmd-2020-72
- Ralph, F. M., Coleman, T., Neiman, P. J., Zamora, R. J., & Dettinger, M. D. (2013, apr). Observed Impacts of Duration and Seasonality of Atmospheric-River Landfalls on Soil Moisture and Runoff in Coastal Northern California. *Journal of Hydrometeorology*, 14(2), 443–459. Retrieved from <https://journals.ametsoc.org/jhm/article/14/2/443/5819/Observed-Impacts-of-Duration-and-Seasonality-of> doi: 10.1175/JHM-D-12-076.1
- Ralph, F. M., Dettinger, M., Lavers, D., Gorodetskaya, I. V., Martin, A., Viale, M., ... Cordeira, J. (2017). Atmospheric rivers emerge as a global science and applications focus. *Bulletin of the American Meteorological Society*, 98(9), 1969–1973. doi: 10.1175/BAMS-D-16-0262.1
- Ralph, F. M., Dettinger, M. D., Cairns, M. M., Galarneau, T. J., & Eylander, J. (2018, apr). Defining “Atmospheric River”: How the Glossary of Meteorology Helped Resolve a Debate. *Bulletin of the American Meteorological Society*, 99(4), 837–839. Retrieved from <http://journals.ametsoc.org/doi/10.1175/BAMS-D-17-0157.1> doi: 10.1175/BAMS-D-17-0157.1
- Ralph, F. M., Neiman, P. J., & Rotunno, R. (2005). Dropsonde observations in low-level jets over the northeastern Pacific Ocean from CALJET-1998 and PACJET-2001: Mean vertical-profile and atmospheric-river characteristics.

- 952 *Monthly Weather Review*, 133(4), 889–910. doi: 10.1175/MWR2896.1
- 953 Ralph, F. M., Neiman, P. J., & Wick, G. A. (2004). Satellite and CALJET aircraft
954 observations of atmospheric rivers over the Eastern North Pacific Ocean during
955 the winter of 1997/98. *Monthly Weather Review*, 132(7), 1721–1745. doi:
956 10.1175/1520-0493(2004)132<1721:SACAOO>2.0.CO;2
- 957 Ralph, F. M., Rutz, J. J., Cordeira, J. M., Dettinger, M., Anderson, M., Reynolds,
958 D., ... Smallcomb, C. (2019, feb). A Scale to Characterize the Strength and
959 Impacts of Atmospheric Rivers. *Bulletin of the American Meteorological Soci-*
960 *ety*, 100(2), 269–289. Retrieved from [https://journals.ametsoc.org/bams/
961 article/100/2/269/69196/A-Scale-to-Characterize-the-Strength-and
962 -Impacts](https://journals.ametsoc.org/bams/article/100/2/269/69196/A-Scale-to-Characterize-the-Strength-and-Impacts) doi: 10.1175/BAMS-D-18-0023.1
- 963 Ralph, F. M., Wilson, A. M., Shulgina, T., Kawzenuk, B., Sellars, S., Rutz, J. J., ...
964 Wick, G. A. (2019, apr). ARTMIP-early start comparison of atmospheric river
965 detection tools: how many atmospheric rivers hit northern California’s Russian
966 River watershed? *Climate Dynamics*, 52(7-8), 4973–4994. Retrieved from
967 <https://doi.org/10.1007/s00382-018-4427-5>, [http://link.springer
968 .com/10.1007/s00382-018-4427-5](http://link.springer.com/10.1007/s00382-018-4427-5) doi: 10.1007/s00382-018-4427-5
- 969 Ramos, A. M., Blamey, R. C., Algarra, I., Nieto, R., Gimeno, L., Tomé, R., ...
970 Trigo, R. M. (2019). From amazonia to southern africa: atmospheric mois-
971 ture transport through low-level jets and atmospheric rivers. *Annals of the
972 New York Academy of Sciences*, 1436(1), 217-230. Retrieved from [https://
973 nyaspubs.onlinelibrary.wiley.com/doi/abs/10.1111/nyas.13960](https://nyaspubs.onlinelibrary.wiley.com/doi/abs/10.1111/nyas.13960) doi:
974 10.1111/nyas.13960
- 975 Ramos, A. M., Tomé, R., Trigo, R. M., Liberato, M. L., & Pinto, J. G. (2016,
976 sep). Projected changes in atmospheric rivers affecting Europe in CMIP5
977 models. *Geophysical Research Letters*, 43(17), 9315–9323. Retrieved from
978 <https://doi.org/10.1002/2016GL070634>[http://doi.wiley.com/10.1002/
979 2016GL070634](http://doi.wiley.com/10.1002/2016GL070634) doi: 10.1002/2016GL070634
- 980 Ramos, A. M., Trigo, R. M., Liberato, M. L. R., & Tomé, R. (2015, apr). Daily
981 Precipitation Extreme Events in the Iberian Peninsula and Its Associa-
982 tion with Atmospheric Rivers*. *Journal of Hydrometeorology*, 16(2), 579–
983 597. Retrieved from [https://journals.ametsoc.org/jhm/article/16/2/
984 579/6106/Daily-Precipitation-Extreme-Events-in-the-Iberian](https://journals.ametsoc.org/jhm/article/16/2/579/6106/Daily-Precipitation-Extreme-Events-in-the-Iberian) doi:
985 10.1175/JHM-D-14-0103.1
- 986 Rasmusson, E. M., & Arkin, P. A. (1993, aug). A Global View of Large-Scale Pre-
987 cipitation Variability. *Journal of Climate*, 6(8), 1495–1522. Retrieved from
988 [http://journals.ametsoc.org/doi/10.1175/1520-0442\(1993\)006%3C1495:
989 AGVOLS%3E2.0.CO;2](http://journals.ametsoc.org/doi/10.1175/1520-0442(1993)006%3C1495:AGVOLS%3E2.0.CO;2) doi: 10.1175/1520-0442(1993)006<1495:AGVOLS>2.0.CO;
990 2
- 991 Reid, K. J., King, A. D., Lane, T. P., & Short, E. (2020). The Sensitivity of Atmo-
992 spheric River Identification to Integrated Water Vapor Transport Threshold,
993 Resolution, and Regridding Method. *Journal of Geophysical Research: Atmo-*
994 *spheres*, 125(20), 1–15. doi: 10.1029/2020JD032897
- 995 Rhoades, A. M., Jones, A. D., O’Brien, T. A., O’Brien, J. P., Ullrich, P. A., &
996 Zarzycki, C. M. (2020). Influences of North Pacific Ocean Domain Extent
997 on the Western U.S. Winter Hydroclimatology in Variable-Resolution CESM.
998 *Journal of Geophysical Research: Atmospheres*, 125(14), e2019JD031977.
999 Retrieved from [https://agupubs.onlinelibrary.wiley.com/doi/abs/
1000 10.1029/2019JD031977](https://agupubs.onlinelibrary.wiley.com/doi/abs/10.1029/2019JD031977) (e2019JD031977 10.1029/2019JD031977) doi:
1001 10.1029/2019JD031977
- 1002 Rhoades, A. M., Jones, A. D., Srivastava, A., Huang, H., O’Brien, T. A., Patri-
1003 cola, C. M., ... Zhou, Y. (2020). The Shifting Scales of Western U.S.
1004 Landfalling Atmospheric Rivers Under Climate Change. *Geophysical
1005 Research Letters*, 47(17), e2020GL089096. Retrieved from [https://
1006 agupubs.onlinelibrary.wiley.com/doi/abs/10.1029/2020GL089096](https://agupubs.onlinelibrary.wiley.com/doi/abs/10.1029/2020GL089096)

- 1007 (e2020GL089096 10.1029/2020GL089096) doi: <https://doi.org/10.1029/>
1008 2020GL089096
- 1009 Rhoades, A. M., Risser, M. D., Stone, D. A., Wehner, M. F., & Jones, A. D. (2021).
1010 Implications of warming on western United States landfalling atmospheric
1011 rivers and their flood damages. *Weather and Climate Extremes*, *32*, 100326.
1012 Retrieved from [https://www.sciencedirect.com/science/article/pii/](https://www.sciencedirect.com/science/article/pii/S2212094721000244)
1013 [S2212094721000244](https://www.sciencedirect.com/science/article/pii/S2212094721000244) doi: <https://doi.org/10.1016/j.wace.2021.100326>
- 1014 Rutz, J. J., James Steenburgh, W., & Martin Ralph, F. (2014, feb). Clima-
1015 tological characteristics of atmospheric rivers and their inland penetration
1016 over the western united states. *Monthly Weather Review*, *142*(2), 905–
1017 921. Retrieved from [https://journals.ametsoc.org/mwr/article/142/](https://journals.ametsoc.org/mwr/article/142/2/905/71947/Climatological-Characteristics-of-Atmospheric)
1018 [2/905/71947/Climatological-Characteristics-of-Atmospheric](https://journals.ametsoc.org/mwr/article/142/2/905/71947/Climatological-Characteristics-of-Atmospheric) doi:
1019 [10.1175/MWR-D-13-00168.1](https://doi.org/10.1175/MWR-D-13-00168.1)
- 1020 Rutz, J. J., Shields, C. A., Lora, J. M., Payne, A. E., Guan, B., Ullrich, P., ...
1021 Viale, M. (2019, dec). The Atmospheric River Tracking Method Inter-
1022 comparison Project (ARTMIP): Quantifying Uncertainties in Atmospheric
1023 River Climatology. *Journal of Geophysical Research: Atmospheres*, *124*(24),
1024 13777–13802. Retrieved from [https://onlinelibrary.wiley.com/doi/abs/](https://onlinelibrary.wiley.com/doi/abs/10.1029/2019JD030936)
1025 [10.1029/2019JD030936](https://onlinelibrary.wiley.com/doi/abs/10.1029/2019JD030936) doi: [10.1029/2019JD030936](https://doi.org/10.1029/2019JD030936)
- 1026 Shearer, E. J., Nguyen, P., Sellars, S. L., Analui, B., Kawzenuk, B., Hsu, K.-l., &
1027 Sorooshian, S. (2020). Examination of global midlatitude atmospheric river
1028 lifecycles using an object-oriented methodology. *Journal of Geophysical Re-*
1029 *search: Atmospheres*, *125*(22), e2020JD033425. Retrieved from [https://](https://agupubs.onlinelibrary.wiley.com/doi/abs/10.1029/2020JD033425)
1030 agupubs.onlinelibrary.wiley.com/doi/abs/10.1029/2020JD033425 doi:
1031 <https://doi.org/10.1029/2020JD033425>
- 1032 Shields, C. A., & Kiehl, J. T. (2016a, aug). Atmospheric river landfall-latitude
1033 changes in future climate simulations. *Geophysical Research Letters*, *43*(16),
1034 8775–8782. Retrieved from <http://doi.wiley.com/10.1002/2016GL070470>
1035 doi: [10.1002/2016GL070470](https://doi.org/10.1002/2016GL070470)
- 1036 Shields, C. A., & Kiehl, J. T. (2016b, jul). Simulating the Pineapple Express in the
1037 half degree Community Climate System Model, CCSM4. *Geophysical Research*
1038 *Letters*, *43*(14), 7767–7773. Retrieved from [http://doi.wiley.com/10.1002/](http://doi.wiley.com/10.1002/2016GL069476)
1039 [2016GL069476](http://doi.wiley.com/10.1002/2016GL069476) doi: [10.1002/2016GL069476](https://doi.org/10.1002/2016GL069476)
- 1040 Shields, C. A., Rosenbloom, N., Bates, S., Hannay, C., Hu, A., Payne, A. E., ...
1041 Truesdale, J. (2019). Meridional Heat Transport During Atmospheric Rivers
1042 in High-Resolution CESM Climate Projections. *Geophysical Research Letters*,
1043 *46*(24), 14702–14712. doi: [10.1029/2019GL085565](https://doi.org/10.1029/2019GL085565)
- 1044 Shields, C. A., Rutz, J. J., Leung, L. R., Ralph, F. M., Wehner, M., O'Brien, T.,
1045 & Pierce, R. (2019, feb). Defining Uncertainties through Comparison of At-
1046 mospheric River Tracking Methods. *Bulletin of the American Meteorological*
1047 *Society*, *100*(2), ES93–ES96. Retrieved from [http://journals.ametsoc.org/](http://journals.ametsoc.org/doi/10.1175/BAMS-D-18-0200.1)
1048 [doi/10.1175/BAMS-D-18-0200.1](http://journals.ametsoc.org/doi/10.1175/BAMS-D-18-0200.1) doi: [10.1175/BAMS-D-18-0200.1](https://doi.org/10.1175/BAMS-D-18-0200.1)
- 1049 Shields, C. A., Rutz, J. J., Leung, L.-Y., Ralph, F. M., Wehner, M., Kawzenuk,
1050 B., ... Nguyen, P. (2018, jun). Atmospheric River Tracking Method
1051 Intercomparison Project (ARTMIP): project goals and experimental de-
1052 sign. *Geoscientific Model Development*, *11*(6), 2455–2474. Retrieved from
1053 <https://www.geosci-model-dev.net/11/2455/2018/> doi: [10.5194/](https://doi.org/10.5194/gmd-11-2455-2018)
1054 [gmd-11-2455-2018](https://doi.org/10.5194/gmd-11-2455-2018)
- 1055 Skinner, C. B., Lora, J. M., Payne, A. E., & Poulsen, C. J. (2020). Atmo-
1056 spheric river changes shaped mid-latitude hydroclimate since the mid-
1057 holocene. *Earth and Planetary Science Letters*, *541*, 116293. Retrieved from
1058 <http://www.sciencedirect.com/science/article/pii/S0012821X20302363>
1059 doi: <https://doi.org/10.1016/j.epsl.2020.116293>
- 1060 Sousa, P. M., Ramos, A. M., Raible, C. C., Messmer, M., Tomé, R., Pinto, J. G.,
1061 & Trigo, R. M. (2020, 12). North Atlantic Integrated Water Vapor Trans-

- 1062 port—From 850 to 2100 CE: Impacts on Western European Rainfall. *Journal*
1063 *of Climate*, 33(1), 263–279. Retrieved from [https://doi.org/10.1175/](https://doi.org/10.1175/JCLI-D-19-0348.1)
1064 [JCLI-D-19-0348.1](https://doi.org/10.1175/JCLI-D-19-0348.1) doi: 10.1175/JCLI-D-19-0348.1
- 1065 Stohl, A., Forster, C., & Sodemann, H. (2008). Remote sources of water vapor
1066 forming precipitation on the Norwegian west coast at 60°N - A tale of hurri-
1067 canes and an atmospheric river. *Journal of Geophysical Research Atmospheres*,
1068 113(5), 1–13. Retrieved from <http://dx.doi.org/10.1029/2007JD009006>
1069 doi: 10.1029/2007JD009006
- 1070 Taylor, K. E. (2001, apr). Summarizing multiple aspects of model performance
1071 in a single diagram. *Journal of Geophysical Research: Atmospheres*, 106(D7),
1072 7183–7192. Retrieved from <http://doi.wiley.com/10.1029/2000JD900719>
1073 doi: 10.1029/2000JD900719
- 1074 Taylor, K. E., Stouffer, R. J., & Meehl, G. A. (2012). An overview of CMIP5 and
1075 the experiment design. *Bulletin of the American Meteorological Society*, 93(4),
1076 485–498. doi: 10.1175/BAMS-D-11-00094.1
- 1077 Thepenir, R.-M., & Cruette, D. (1981, oct). Formation of Cloud Bands Associ-
1078 ated with the American Subtropical Jet Stream and Their Interaction with
1079 Midlatitude Synoptic Disturbances Reaching Europe. *Monthly Weather Re-*
1080 *view*, 109(10), 2209–2220. Retrieved from [http://journals.ametsoc.org/](http://journals.ametsoc.org/doi/10.1175/1520-0493(1981)109%3C2209:FOCBAW%3E2.0.CO;2)
1081 [doi/10.1175/1520-0493\(1981\)109%3C2209:FOCBAW%3E2.0.CO;2](http://journals.ametsoc.org/doi/10.1175/1520-0493(1981)109%3C2209:FOCBAW%3E2.0.CO;2) doi:
1082 10.1175/1520-0493(1981)109%3C2209:FOCBAW%3E2.0.CO;2
- 1083 Tilinina, N., Gulev, S. K., Rudeva, I., & Koltermann, P. (2013, sep). Comparing
1084 Cyclone Life Cycle Characteristics and Their Interannual Variability in Dif-
1085 ferent Reanalyses. *Journal of Climate*, 26(17), 6419–6438. Retrieved from
1086 <http://journals.ametsoc.org/doi/10.1175/JCLI-D-12-00777.1> doi:
1087 10.1175/JCLI-D-12-00777.1
- 1088 Ullrich, P. A., & Zarzycki, C. M. (2017, mar). TempestExtremes: a frame-
1089 work for scale-insensitive pointwise feature tracking on unstructured
1090 grids. *Geoscientific Model Development*, 10(3), 1069–1090. Retrieved
1091 from <https://gmd.copernicus.org/articles/10/1069/2017/> doi:
1092 10.5194/gmd-10-1069-2017
- 1093 Viale, M., & Nuñez, M. N. (2011). Climatology of winter orographic precipi-
1094 tation over the subtropical central Andes and associated synoptic and re-
1095 gional characteristics. *Journal of Hydrometeorology*, 12(4), 481–507. doi:
1096 10.1175/2010JHM1284.1
- 1097 Waliser, D. E., Moncrieff, M. W., Burridge, D., Fink, A. H., Gochis, D., Goswami,
1098 B. N., ... Yuter, S. (2012, aug). The “Year” of Tropical Convection (May
1099 2008–April 2010): Climate Variability and Weather Highlights. *Bulletin*
1100 *of the American Meteorological Society*, 93(8), 1189–1218. Retrieved from
1101 <http://journals.ametsoc.org/doi/abs/10.1175/2011BAMS3095.1> doi:
1102 10.1175/2011BAMS3095.1
- 1103 Warner, M. D., Mass, C. F., & Salathé, E. P. (2015). Changes in Winter At-
1104 mospheric Rivers along the North American West Coast in CMIP5 Climate
1105 Models. *Journal of Hydrometeorology*, 16(1), 118–128. Retrieved from
1106 <http://journals.ametsoc.org/doi/10.1175/JHM-D-14-0080.1> doi:
1107 10.1175/JHM-D-14-0080.1
- 1108 Warner, M. D., Mass, C. F., & Salathé, E. P. (2012). Wintertime extreme
1109 precipitation events along the Pacific Northwest Coast: Climatology and
1110 synoptic evolution. *Monthly Weather Review*, 140(7), 2021–2043. doi:
1111 10.1175/MWR-D-11-00197.1
- 1112 Wille, J. D., Favier, V., Dufour, A., Gorodetskaya, I. V., Turner, J., Agosta, C.,
1113 & Codron, F. (2019). West Antarctic surface melt triggered by atmo-
1114 spheric rivers. *Nature Geoscience*, 12(11), 911–916. Retrieved from [http://](http://dx.doi.org/10.1038/s41561-019-0460-1)
1115 dx.doi.org/10.1038/s41561-019-0460-1 doi: 10.1038/s41561-019-0460-1
- 1116 Wille, J. D., Favier, V., Gorodetskaya, I. V., Agosta, C., Kittel, C., Beeman, J. C.,

1117 ... Codron, F. (2021). Antarctic atmospheric river climatology and pre-
1118 cipitation impacts. *Journal of Geophysical Research: Atmospheres*, 126(8),
1119 e2020JD033788. Retrieved from [https://agupubs.onlinelibrary.wiley](https://agupubs.onlinelibrary.wiley.com/doi/abs/10.1029/2020JD033788)
1120 [.com/doi/abs/10.1029/2020JD033788](https://doi.org/10.1029/2020JD033788) (e2020JD033788 2020JD033788) doi:
1121 <https://doi.org/10.1029/2020JD033788>

1122 Xin, X., Wu, T., Shi, X., Zhang, F., Li, J., Chu, M., ... Wei, M. (2019). *BCC*
1123 *BCC-CSM2MR model output prepared for CMIP6 ScenarioMIP ssp585*. Earth
1124 System Grid Federation. Retrieved from [https://doi.org/10.22033/ESGF/](https://doi.org/10.22033/ESGF/CMIP6.3050)
1125 [CMIP6.3050](https://doi.org/10.22033/ESGF/CMIP6.3050) (Version 20190125) doi: 10.22033/ESGF/CMIP6.3050

1126 Yukimoto, S., Koshiro, T., Kawai, H., Oshima, N., Yoshida, K., Urakawa, S., ...
1127 Adachi, Y. (2019). *MRI MRI-ESM2.0 model output prepared for CMIP6*
1128 *ScenarioMIP ssp585*. Earth System Grid Federation. Retrieved from
1129 <https://doi.org/10.22033/ESGF/CMIP6.6929> (Version 20190625) doi:
1130 [10.22033/ESGF/CMIP6.6929](https://doi.org/10.22033/ESGF/CMIP6.6929)

1131 Zhang, Z., Ralph, F. M., & Zheng, M. (2019). The Relationship Between Extratrop-
1132 ical Cyclone Strength and Atmospheric River Intensity and Position. *Geophys-
1133 ical Research Letters*, 46(3), 1814–1823. doi: 10.1029/2018GL079071

1134 Zhou, Y., O'Brien, T. A., Ullrich, P. A., Collins, W. D., Patricola, C. M., &
1135 Rhoades, A. M. (2021, apr). Uncertainties in Atmospheric River Life-
1136 cycles by Detection Algorithms: Climatology and Variability. *Journal*
1137 *of Geophysical Research: Atmospheres*, 126(8), 1–22. Retrieved from
1138 <https://onlinelibrary.wiley.com/doi/10.1029/2020JD033711> doi:
1139 [10.1029/2020JD033711](https://doi.org/10.1029/2020JD033711)

1140 Zhu, Y., & Newell, R. E. (1998, mar). A Proposed Algorithm for Moisture
1141 Fluxes from Atmospheric Rivers. *Monthly Weather Review*, 126(3), 725–
1142 735. Retrieved from [http://journals.ametsoc.org/doi/abs/10.1175/1520-](http://journals.ametsoc.org/doi/abs/10.1175/1520-0493(1998)126<0725:APAFMF>2.0.CO;2)
1143 [-0493\(1998\)126<0725:APAFMF>2.0.CO;2](http://journals.ametsoc.org/doi/abs/10.1175/1520-0493(1998)126<0725:APAFMF>2.0.CO;2)
1144 doi: 10.1175/1520-0493(1998)126(0725:APAFMF)2.0.CO;2

Supporting Information for “Increases in Future AR Count and Size: Overview of the ARTMIP Tier 2 CMIP5/6 Experiment”

T. A. O’Brien^{1,2} *, M. F. Wehner³ and A. E. Payne⁴ and C. A. Shields⁵ and
J. J. Rutz⁶ and L.-R. Leung⁷ and F. M. Ralph⁸ and A. Collopy^{9,10} and
I. Gorodetskaya¹¹ and B. Guan¹² and J. M. Lora¹³ and E. McClenny¹⁴ and
K. M. Nardi¹⁵ and A. M. Ramos¹⁶ and R. Tomé¹⁷ and C. Sarangi^{7,18} and
E. J. Shearer¹⁷ and P. A. Ullrich¹⁴ and C. Zarzycki¹⁵ and B. Loring³ and
H. Huang² and H. A. Inda-Díaz^{14,2} and A. M. Rhoades² and Y. Zhou²

¹Dept. of Earth and Atmospheric Sciences, Indiana University, Bloomington, IN, USA

²Climate and Ecosystem Sciences Division, Lawrence Berkeley National Laboratory, Berkeley, CA, USA

³Computational Research Division, Lawrence Berkeley National Laboratory, Berkeley, CA, USA

⁴Dept. of Earth and Space Sciences, University of Michigan, Ann Arbor, MI, USA

⁵National Center for Atmospheric Research, Boulder, CO, USA

⁶National Weather Service, Western Region Headquarters, Science and Technology Infusion Division, Salt Lake City, UT, USA

⁷Atmospheric Sciences and Global Change Division, Pacific Northwest National Laboratory, Richland, WA, USA

⁸Center for Western Weather and Water Extremes, Scripps Institution of Oceanography, University of California, San Diego, La
Jolla, CA, USA

⁹Universities Space Research Association, Columbia, MD, USA

¹⁰Global Modeling and Assimilation Office, NASA Goddard Space Flight Center, Greenbelt, MD, USA

¹¹Centre for Environmental and Marine Studies, Dept. of Physics, University of Aveiro, Portugal

¹²Joint Institute for Regional Earth System Science and Engineering, University of California, Los Angeles, CA, USA

¹³Dept. of Earth and Planetary Sciences, Yale University, New Haven, CT, USA

December 15, 2021, 6:41am

¹⁴Dept. of Land, Air and Water Resources, University of California, Davis, Davis, CA, USA

¹⁵Dept. of Meteorology and Atmospheric Science, Penn State University, University Park, PA, USA

¹⁶Instituto Dom Luiz (IDL), Faculdade de Ciências, Universidade de Lisboa, Lisboa, Portugal

¹⁷Center for Hydrometeorology and Remote Sensing, University of California, Irvine, Irvine, CA, USA

¹⁸Department of Civil Engineering, Indian Institute of Technology Madras, India

Contents of this file

1. Text S1 to S4

2. Figures S1 to S5

3. Table S1

Introduction

This supplemental information provides additional useful details on ARDTs, their treatment of thresholds, and our grouping of ARDTs into categories. The supplemental figures expand on figures in the main text to show all ARDT-simulation combinations.

Text S1.

Treatment of Thresholds

Corresponding author: T. A. O'Brien, Department of Earth and Atmospheric Sciences, Indiana University, 1001 E. 10th Street, Bloomington, IN 47408, USA (obrienta@iu.edu)

*Dept. of Earth and Atmospheric Science,
1001 E. 10th St, Bloomington, IN, 47408

33 We document here choices/specializations (if any) that ARDT contributors made in
34 running their ARDTs on the Tier 2 CMIP5/6 simulations

- 35 • `ARCONNECT_v2`: only uses absolute threshold; no Tier 2-specific decisions needed
- 36 • `Guan_Waliser_v2`: uses 85th percentile from the historical simulation
- 37 • `IDL_rel_future`: uses 85th percentile calculated from the future simulation
- 38 • `IDL_rel_hist`: uses 85th percentile calculated from the historical simulation
- 39 • `Lora_v2`: uses a time-and-latitude dependent IVT threshold that asymptotes to 225
40 kg/m/s at the poles; the time/latitude dependence of the threshold is a function of the
41 30-day running mean and a zonal average of IWV, so no Tier 2-specific decisions are
42 needed
- 43 • `Mundhenk_v3`: calculates the mean and seasonal cycle of IVT based on the historical
44 simulation and removes this to determine the IVT anomaly relative to the historical period
- 45 • `PNNL_v1`: only uses absolute threshold; no Tier 2-specific decisions needed
- 46 • `TECA_BARD_v1.0.1`: uses threshold relative to spatial map of IVT at a given time;
47 no Tier 2-specific decisions needed

48 The `Mundhenk_v3` algorithm differs from prior published versions (i.e., `Mundhenk_v1`,
49 `Mundhenk_v2`) in its more reliable detection of AR objects that cross the boundary of the
50 dataset's spatial domain.

51 The `Tempest` ARDT uses an absolute threshold for the laplacian of IVT. The Tier
52 1 version also utilized an absolute threshold of 250 kg/m/s of IVT, but it was later
53 determined that this threshold had no effect on the ARDT results because regions that
54 satisfied the Laplacian threshold also satisfied the IVT threshold. The minimum latitude
55 for ARs was raised to 20°, from 15°, to filter easterly waves. The stencil radius and

56 magnitude used for the Laplacian depends on the model grid, and this is held constant
57 for the historical and future simulations.

58 Discussions with the **Tempest** contributing scientists indicate that the algorithm may
59 benefit from further tuning of their method when applied to moderately low resolution
60 data, and efforts are underway to provide a second version of their contribution to Tier
61 2. Such discoveries and improvements are a benefit of intercomparison projects.

62 **Text S2.**

63 **Classification of ARDTs**

64 Building on Rutz et al. (2019), we classify the Tier 2 CMIP5/6 ARDTs into three
65 groups, based on their treatment of thresholds: *absolute*, *fixed relative*, and *relative*. These
66 classifications are indicated as *abs.*, *fix. rel.*, and *rel.* in Table S1. A key motivation for
67 this categorization is aggregating ARDTs by their sensitivity to thermodynamic changes
68 in IVT, with the assumption that ARDTs employing absolute thresholds to moisture fields
69 will be the most sensitive, and ARDTs employing time-dependent thresholds will be least
70 sensitive.

71 **Absolute ARDTs:** We define *absolute ARDTs* as utilizing any fixed thresholds (e.g.,
72 in IVT) for discriminating ARs from the background. **ARCONNECT_v2** and **PNNL_v1** unam-
73 biguously fit in this category. **Lora_v2** uses an IVT threshold that varies with latitude and
74 time, and the threshold asymptotes to 250 kg/m/s at mid-to-high latitudes (the thresh-
75 old increases toward infinity approaching the tropics). This design effectively imposes an
76 absolute threshold of at least 250 kg/m/s. Because of this, we classify **Lora_v2** as an
77 *absolute ARDT*, while recognizing that this is not a perfect categorization.

78 **Fixed relative ARDTs:** We define *fixed relative ARDTs* as those that employ relative
79 thresholds that do not vary with time. For example, `Guan_Waliser_v2` calculates the 85th
80 percentile of IVT from the historical simulations and discriminates ARs from the back-
81 ground where IVT is greater than the local, historical 85th percentile; hence the threshold
82 used in the `Guan_Waliser_v2` algorithm does not change in time. The `IDL_rel_hist`
83 and `IDL_rel_future` ARDTs use a similar approach and are therefore also categorized
84 as *fixed relative ARDTs*. `Mundhenk_v3` calculates IVT anomalies relative to the historical
85 period and identifies ARs that are above the 94th percentile of the historical simulation,
86 so it also fits unambiguously in the *fixed relative* category.

87 **Relative ARDTs:** We define *relative ARDTs* as those that employ relative thresholds
88 that vary with time. `TECA_BARD_v1.01` unambiguously fits into this category, since ARs
89 are identified where IVT is above a fixed percentile of IVT, where the percentile is calcu-
90 lated in space (in contrast to time, e.g., for `Guan_Waliser_v2`). `Tempest` uses an absolute
91 threshold applied to the Laplacian of the IVT field, which might warrant its classification
92 as an absolute ARDT. However, the use of the Laplacian removes the mean of the IVT
93 field; therefore `Tempest` identifies areas of IVT that are high relative to nearby areas of
94 IVT at the same timestep. We therefore classify `Tempest` as a *relative ARDT*.

95 **Text S3.**

96 **Details on Missing Data** All ARDTs detect ARs for the 1951-2099 period for the
97 combined historical and future simulations for each CMIP5/6 model. We analyze output
98 from the entire 1951-2099 timeperiod. There are some exceptions to this: output from the
99 CMIP6 IPSL-CM6A-LR SSP5-8.5 simulation are only available through 2049, there are
100 data corruption issues for the year 2006 in the CMIP5 CSIRO-Mk3-6-0 simulation, and

101 there are data corruption issues for the year 2095-2099 for the TECA_BARD_v1.01 output
102 applied to the CMIP5 IPSL-CM5B-LR simulation. Years with data corruption issues
103 are marked as missing, and trends and climatologies are only calculated considering non-
104 missing data. The Guan_Waliser_v2 algorithm did not supply ARDT catalogues for the
105 NorESM1-M and BCC-CSM2-MR simulations due to technical issues at the time.

106 **Text S4.**

107 **Comment on the Tier 2 Reanalysis Experiment**

108 The tiered structure of the ARTMIP experiments requires that all participants con-
109 tribute to the Tier 1 experiment; by design, all ARDTs participating in the Tier 2
110 CMIP5/6 experiment also have been run on MERRA-2 as part of the Tier 1 experiment.
111 A separate ARTMIP Tier 2 experiment is currently underway, comparing ARDT results
112 applied to different reanalyses. The set of ARDTs participating in the Tier 2 Reanalysis
113 experiment is not identical to the set participating in this Tier 2 CMIP5/6 experiment,
114 so use of multiple reanalyses is not possible for ARDTs. For the sake of uniformity in the
115 experimental approach, we use only the MERRA-2 reanalysis. Preliminary analysis of
116 the Tier 2 Reanalysis experiment (not shown) indicates that the uncertainties associated
117 with choice of reanalysis are small compared to the uncertainties discussed in this paper,
118 and it is therefore unlikely that use of a different reanalysis would change the qualitative
119 conclusions of this paper.

Table S1. (left) ARDT algorithms, and associated metadata, that contributed to the Tier 2 CMIP5/6 experiment. ARDT classifications ('Class.')

(right) Details of CMIP5/6 models used in the Tier 2 experiment.

ARDTs				Models			
Algorithm ID	Contrib.	Class.	Region	MIP Era	Model Name	Inst.	~Res. [km]
ARCONNECT_v2	Shearer	abs.	Global	CMIP5	CCSM4	NCAR	120
GuanWaliser_v2	Guan	fix. rel.	Global	CMIP5	CSIRO-Mk3-6	CSIRO	207
IDL_rel_future	Ramos	fix. rel.	W. Europe, S. Africa	CMIP5	CanESM2	CCCMA	310
IDL_rel_hist	Ramos	fix. rel.	W. Europe, S. Africa	CMIP5	IPSL-CM5A-LR	IPSL	296
Lora_v2	Lora	abs.	Global	CMIP5	IPSL-CM5B-LR	IPSL	296
Mundhenk_v3	Nardi	fix. rel.	Global	CMIP5	NorESM1-M	NCC	242
PNNL_v1	Sarangi	abs.	W. U.S.	CMIP6	BCC-CSM2-MR	BCC	124
Tempest	McClenny	rel.	Global	CMIP6	IPSL-CM6A-LR	IPSL	198
TECA_BARD_v1.01	O'Brien	rel.	Global	CMIP6	MRI-ESM2-0	MRI	124



Figure S1. Maps of AR frequency (AR days per year) from 1981-2010. Columns correspond to ARs detected by specific ARDTs, and rows correspond to input datasets (MERRA-2 for the first row and CMIP5/6 for other rows). The rightmost column shows the multi-ARDT mean frequency for each model. The bottom row shows the multi-model mean for each ARDT (excluding MERRA-2 from the mean). The bottom right panel shows the multi-ARDT mean frequency (excluding MERRA-2 from the mean).



Figure S2. Maps of AR frequency (AR days per year) from 2070-2099. Columns correspond to ARs detected by specific ARDTs, and rows correspond to CMIP5/6 models. The rightmost column shows the multi-ARDT mean frequency for each model. The bottom row shows the multi-model mean for each ARDT. The bottom right panel shows the multi-model, multi-ARDT mean. The CMIP6 IPSL-CM6A-LR row shows the frequency from the last 30 years of available simulation data (2020-2049).

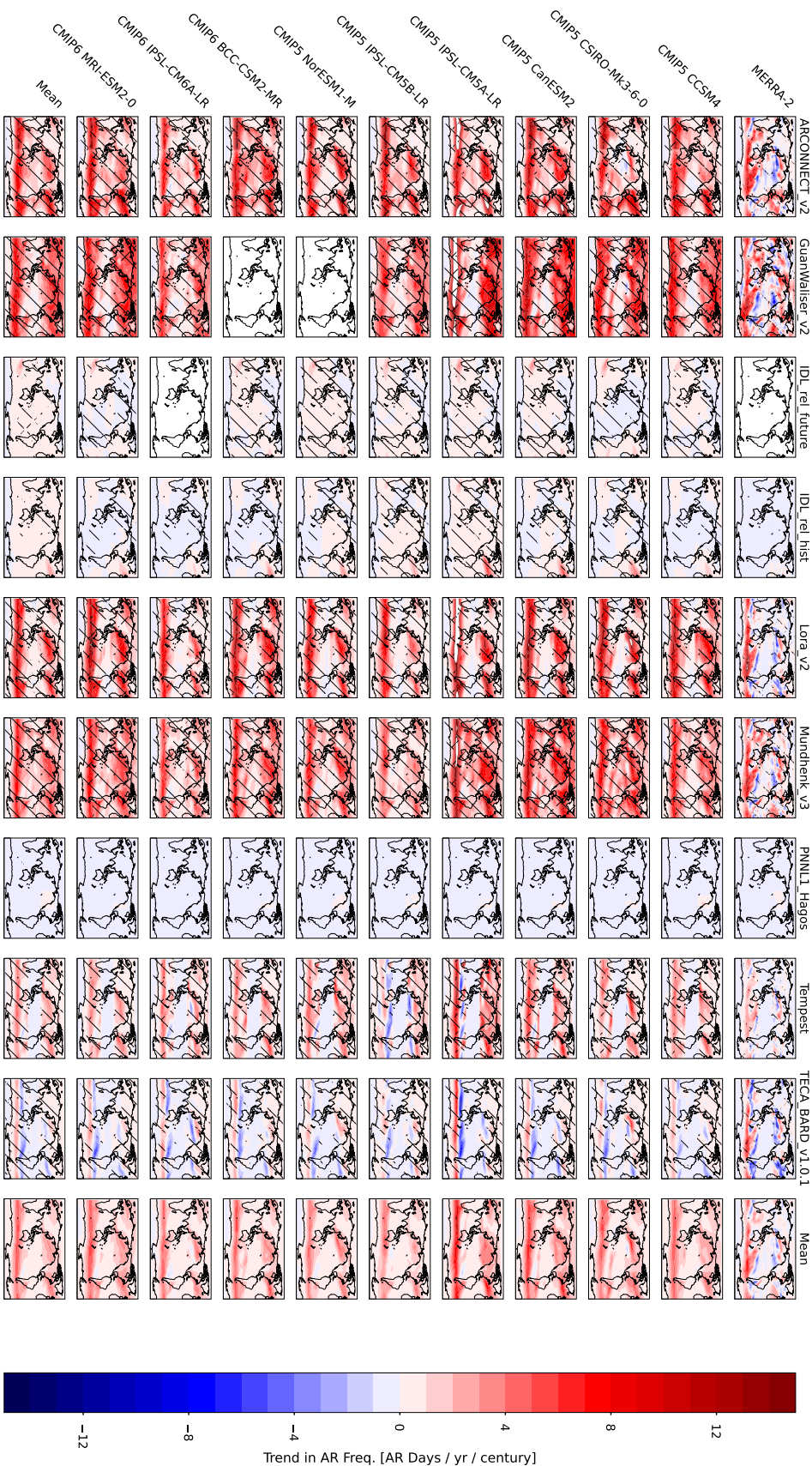


Figure S3. Maps of trends in AR frequency (AR days per year per century) from 1981-2099 (from 1981-2017 for MERRA2). Columns correspond to ARs detected by specific ARDTs, and rows correspond to input datasets (MERRA-2 for the first row and CMIP5/6 for other rows). The rightmost column shows the multi-ARDT mean trend for each model. The bottom row shows the multi-model mean for each ARDT (excluding MERRA-2 from the mean). The bottom right panel shows the multi-model, multi-ARDT mean frequency (excluding MERRA-2 from the mean). Trends for CMIP6 IPSL-CM6A-LR are calculated through 2049.

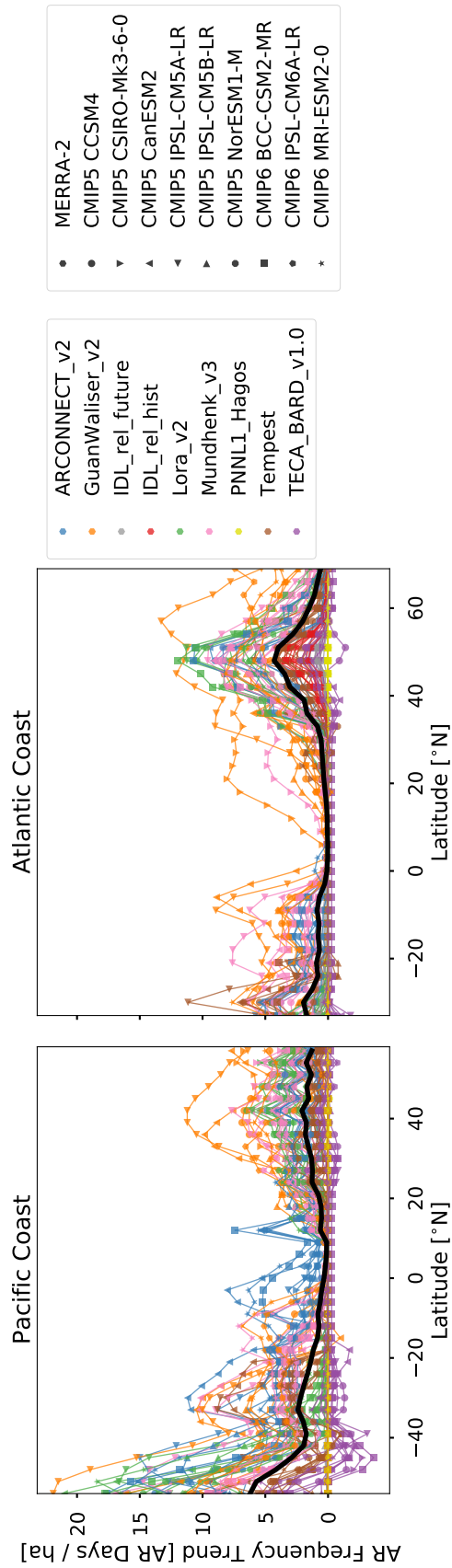


Figure S4. Trends in AR frequency (AR days per year per century) from 1981-2099 for western coastlines along the (a) Pacific and (b) Atlantic oceans. Colors correspond to ARDTs and markers correspond to simulations.

Figure S5. Trends in IVT (a–i), IWV (j–r), and UV≡IVT/IWV (s–A) for each of the CMIP5/6 models, calculated from approximately 1951–2099.

